
CHARACTERIZATION & CALIBRATION OF FORESIGHT™ ICE

Written by: Hareem Nisar

Supervisor: Dr. Terry Peters

Advisor: Dr. Elvis Chen

JULY 8, 2021

ROBARTS RESEARCH INSTITUTE
Western University

Table of Contents

Characterization and Calibration of a 2.5D radial ultrasound.....	2
I. ICE Image Characterization.....	2
Image geometry.....	3
Image Orientation.....	4
Image Data Acquisition.....	5
Image Display Size.....	7
First Scan-Line Consistency	10
Imaging Angle Consistency	14
Image Artifacts.....	14
II. ICE Image Visualization (Slicer-compatible)	17
Volume Reconstruction & Rendering.....	17
Surface Texture mapping	17
DICOM reconstruction and custom interpolation	18
III. ICE Probe Calibration	20
Temporal calibration.....	20
Spatial calibration.....	22
Challenges.....	27
Mitigation.....	28
Characterization of ICE Calibration.....	28
Appendix A.....	34
Code for Conical Volume Reconstruction From a 2D Image.....	34
Code for Texture Mapping an Image to a Cone Model.....	35
Code for Volume Reconstruction from a DICOM file	37

Characterization and Calibration of a 2.5D radial ultrasound

Foresight™ is a recently introduced intracardiac echocardiographic (ICE) probe, designed and manufactured by Conavi Medical Inc. (Toronto, Canada). The Foresight™ ICE probe was invented with a vision of guiding minimally invasive surgeries and cardiovascular interventions. The sophisticated design of the probe includes a single-element ultrasound transducer, which can spin in all 360 degrees as well as tilt physically, thus generating a 2D conical surface ultrasound image lying in 3D space. Due to this unique configuration, we refer to this conical image as 2.5 dimensional. Foresight™ ICE is a catheter-based ultrasound probe which has the unique ability to generate both 2D and 3D imaging, as well as Doppler imaging. This radial design of the probe allows for imaging at multiple views – forward viewing and looking at the sides and constantly switch between multiple views, all without having to move the body of the probe. These features make the Foresight™ ICE probe a rare one-of-its-kind ultrasound catheter with great utility and potential for advanced image guided systems for cardiac interventions. Some potential applications include transseptal puncture guidance, vascular navigation, structural valve repair, localization of valve regurgitation site, and freehand visualization of dynamic anatomical structures. To utilize the Foresight™ ICE probe in the design on an image guided system, the features and behaviors of imaging system need to be understood in depth. In addition, the system needs to be integrated into a tracking environment and ultrasound probe may need to be calibrated. VASST lab at Robarts Research Institute is one of the very early adopters of this technology. In 2017, soon after this novel probe was introduced commercially, we started working with this ultrasound system. As one of the early research users of the Foresight™ ICE probe, many of the parameters essential for enabling the use of this device in an image-guided intervention system, were unknown at that time. Since then, we have done extensive analysis of the imaging system and explored some of the potential applications as well. This paper presents the (I) characterization of the Foresight™ ICE image, (II) multiple ways to visualize the unique 2.5D conical imaging and (III) the process to calibrate the ultrasound probe and use it in a tracking environment. This document is to serve as a starting point and include guidelines to be used by the industrial and research users of a conical ultrasound imaging system.

I. ICE Image Characterization

A forward-looking ICE probe presents numerous opportunities for advanced image guided system designs, holding the potential to simplify and improve the cardiovascular and abdominal transcatheter interventions. To utilize Foresight™ ICE probe in an image guided system based on spatial tracking, it is necessary to understand how the ultrasound image is presented on the screen and the image variability with respect to changing parameters such as depth, imaging angle, frequency, of the ultrasound, as well as inter-variability of image between probes.

In this section we describe experiments to evaluate the appearance of the image on the screen and characterize the display of the 2.5D forward looking ICE probe. In all these experiments data was acquired as real-time screenshots of the console screen using an Epiphan (Epiphan Video, Canada) frame-grabber. The following questions were considered to perform image characterization for the Foresight™ ICE system.

1. **Image Geometry:** How the echogenic data is acquired by the ICE probe? What are the different operating modes the system has to offer?

2. **Image Orientation:** What is the orientation of conical image when displayed as a circle on the console screen?
3. **Image Data Acquisition:** How to acquire imaging data in real time from the console screen?
4. **Image Display Size:** What is the size of the circular image displayed on the console screen? And how it changes with variability in imaging angle and imaging depth? How do these changes compare between probes?
5. **First Scan Line Consistency:** Are the ultrasound images consistent with each other? In other words, does the 12 o'clock position of the radial image always represent the same physical position with respect to the probe?
6. **Imaging Angle Consistency:** What are the factors affecting the value of imaging angle?
7. **Image Artifacts:** What image artifacts are observed, unique to the Foresight™ ICE probe?

Image geometry

The ultrasound imaging acquired through Conavi's Foresight™ ICE probe is a 2-dimensional surface image, in the shape of a cone, lying in 3-dimensional space. We sometimes refer to this original conical surface image as 2.5-dimensional. The hexagonal transducer element transmits and receives a single echo beam. The range or depth of this ultrasonic beam can be controlled and lies between 30mm and 80mm. This parameter is referred to as the *scanning direction*, the *field-of-view* (FOV), or the *radial depth* (r). The unique geometry is attained by the 360-degrees spinning motion of a single-element transducer. One complete spinning motion also referred to as the angular rotation, generates an ultrasound image. In spherical coordinates, this motion is represented by the theta (θ). This parameter is referred to as the *angle of rotation* or *rotational angle* (θ). The transducer element further can tilt in its position, causing the shape of the cone to change. The users have the option to control this tilt angle in multiple ways – manually set a value, continuous change from minimum to maximum tilt angle, and continuous imaging between the pre-set values for tilting. In spherical coordinates, the tilt is represented by the angle phi (ϕ). This parameter is referred to as the *imaging angle* (ϕ) or the *tilt angle*. The schematics of ultrasound acquisition and geometry for Foresight™ ICE imaging can be seen in figure 1.

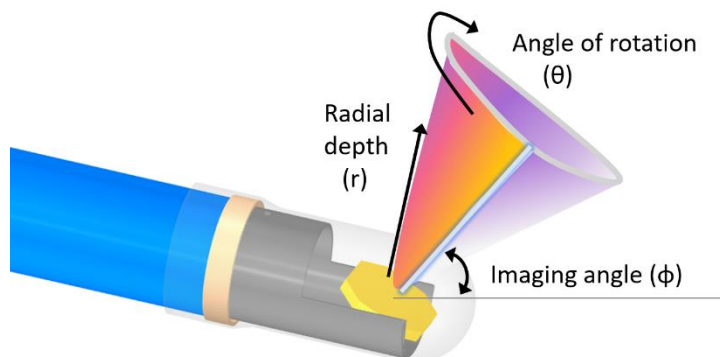


Figure 1 – Ultrasound image acquisition by the Foresight™ ICE probe as a conical geometry

The Foresight™ ICE probe provides a unique opportunity to not only look at all the four sides around the tip of the probe but also look ahead in space using a smaller imaging angle. The ICE probe is said to operate in side-viewing mode when the imaging angle is between 89 and **70 degrees**, and in forward-looking or forward-viewing mode when the imaging angle is less than **70 degrees**. Figure 2 shows an example of the shape of the conical ICE image in the side-viewing and the forward-viewing mode.

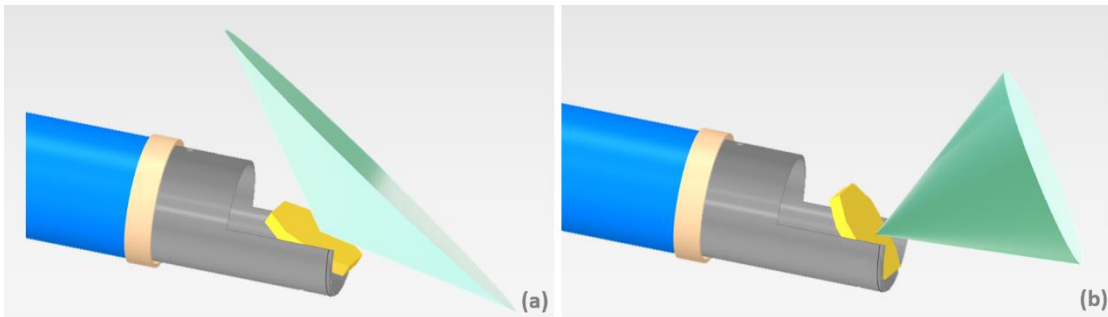


Figure 2 – (a) Side-viewing and (b) forward-viewing modes of Conavi’s Foresight™ ICE probe with larger imaging angle and smaller imaging angle respectively.

Image Orientation

Although the ultrasound images acquired by the Foresight™ ICE probe are 2.5D in nature, they occupy space in all three dimensions. The Hummingbird console includes a traditional flat monitor screen that displays two-dimensional information. Therefore, a question arises of how and in what view is the conical image displayed on the screen.

The 2.5D conical surface image, generated by the Foresight™ ICE probe, is displayed on the 2D monitor screen as a circular image by default. This circular image is the apical view of the conical image, as seen from outside the cone shape. The image can be rotated via touch screen to view the conical surface from different angles. At each of these views, the image is displayed as a parallel projection of the 2.5D conical surface image on the monitor screen. Figure 3(a-d) shows different views of the same ultrasound image where figure 3(d) represents the default or ‘home’ view for that image. When the imaging angle is decreased, the cone becomes more forward-looking and the circular image becomes somewhat smaller in diameter (see figure 3(e,f)).

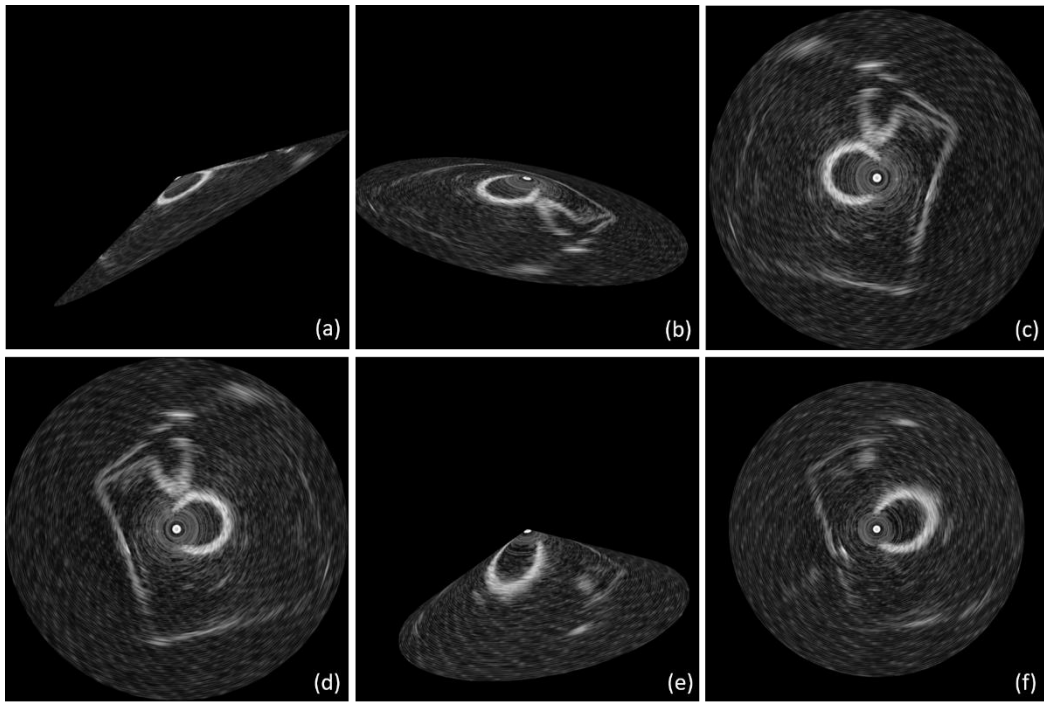


Figure 3 – (a)(b) Different views of conical ICE image in side-viewing mode as seen on Hummingbird console. (c) ICE image view, as seen from inside the cone. (d) Default or ‘Home’ view of the ICE, as seen from the apex of the cone. (e) A forward-looking ICE image at a smaller imaging angle and (d) its default apical view.

Image Data Acquisition

As described earlier, Conavi’s Foresight™ ICE probe acquires the ultrasonic information in shape of a 2D conical surface, displayed on a traditional flat monitor screen as a circle. Though this circular image contains all the necessary anatomical information a clinician might need, it is inherently misleading in terms of spatial arrangement of the viewed anatomy. The system includes an option to rotate the conical image and view the conical ultrasound image from all angles. The “home” button resets the view to the default cone orientation i.e., apical view of the conical image seen from the outside of the cone shape. Figure 4 shows the console layout and highlights the common buttons and parameters to use.

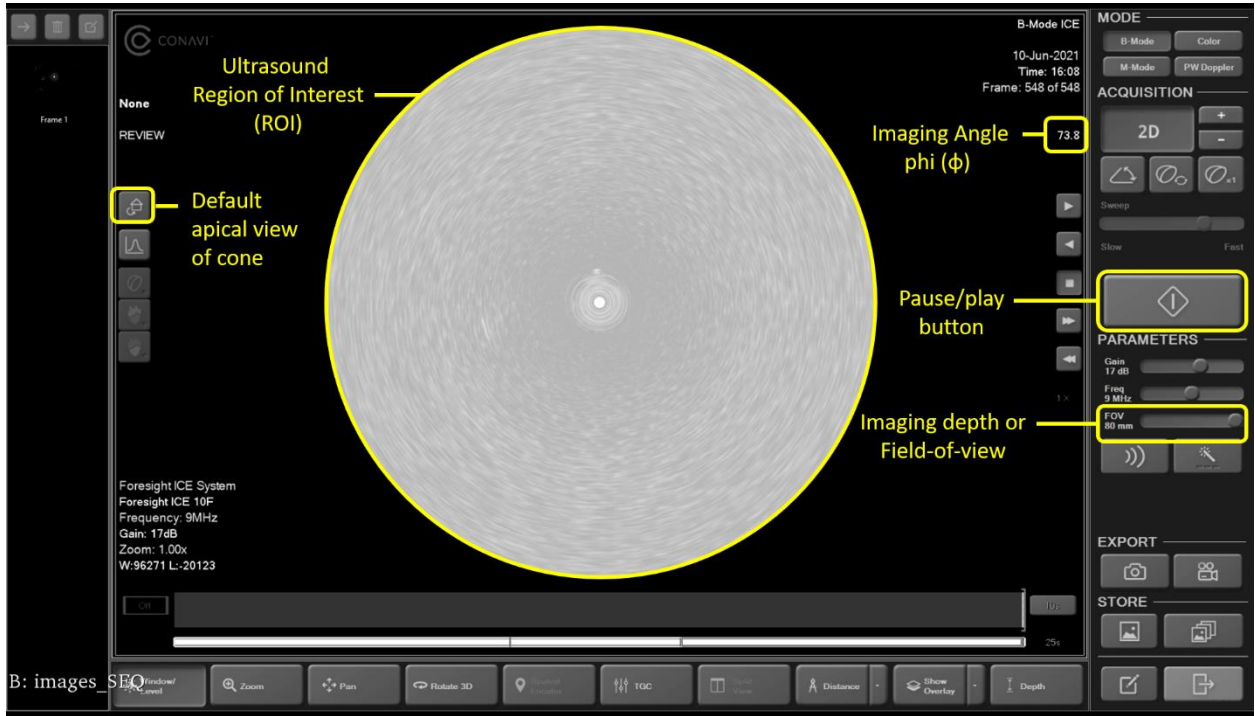


Figure 4 – Screenshot of Conavi’s Hummingbird console, displaying a conical ICE image from the apical view.

As seen in figure 3, different views of the conical image can be seen by rotating the shape on the screen. The angle of the cone itself is controlled by using the (+) and (-) buttons on screen, next to the displayed value of imaging angle. The primary software we have used is called 3D Slicer – an open source platform for medical image processing and visualization. In all our experiments, the ultrasound data are acquired as a screenshot of the console screen in 2D form using a frame-grabber (DVI2USB 3.0, Epiphan Video, USA). The data is transferred to the 3D Slicer environment through a PLUS server application. The imaging angle is extracted from the screen in degrees using an optical character recognition (OCR) algorithm integrated within the PLUS server. The image is cropped to obtain only the circular region-of-interest (ROI). The 2.5D conical information is then reconstructed from the 2D circle images. The circular image (in x, y space) is reconstructed to a conical surface image, lying in 3D space, using the equation below. The schematic of this mathematical conversion is described in figure 5.

$$\begin{bmatrix} x_{3D} \\ y_{3D} \\ z_{3D} \end{bmatrix} = \begin{bmatrix} 1 & 0 & -o_x \\ 0 & 1 & -o_y \\ 0 & 0 & \|(x_{2D}, y_{2D})\| \cdot \tan(90 - \phi) \end{bmatrix} \begin{bmatrix} x_{2D} \\ y_{2D} \\ 1 \end{bmatrix} \quad (1)$$

where ox , oy represents the center of the planar image or the apex of the conical image, and x , y , and z represent the spatial coordinates of imaging pixels. The conical image is reconstructed with the origin of the image set to the apex of the 3D cone image or the center of the 2D circle image.

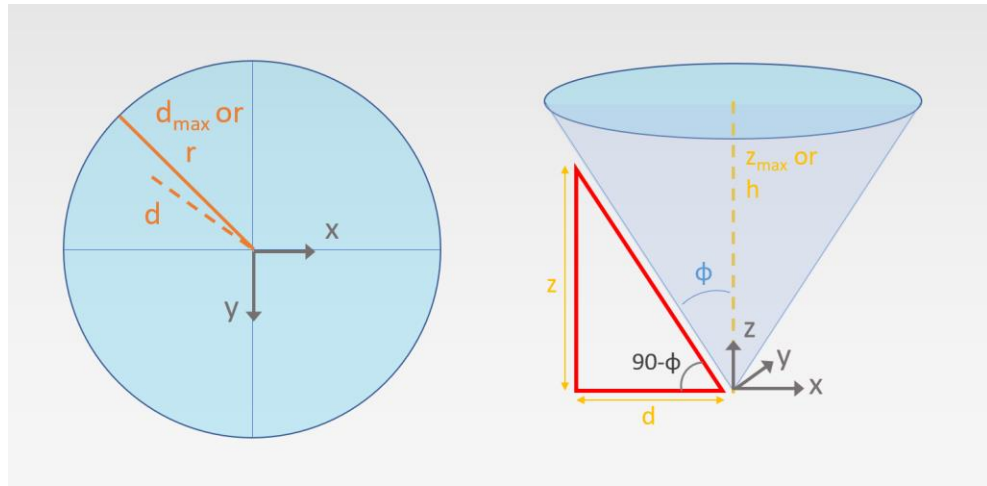


Figure 5 – Reconstruction of the 2.5D conical surface image from a 2D circular image, given a value for imaging angle phi.

Image Display Size

Figure 4 shows a screenshot of the hummingbird console. The screen display includes many controlling parameters including ‘Field of View’ (FOV) and imaging angle, as well as the ultrasound image in a circular shape. This ultrasound-only portion of the image is referred to as the ‘Region of Interest’ or ROI in this study. It was observed that the radius of the ROI is not fixed and changes by variation of imaging angle parameter available in the system. Characterization of this relationship may be required for the design of certain IGS procedures where measurements need to be made outside of the console, in an external software. We aimed to determine and describe this relationship between the size of the ROI and the imaging angle as well as the FOV of the ICE image. Experiments were performed to identify behaviors within a probe as well as to characterize the inter-probe variations in these characteristics.

Methods: To characterize the radial size of the circular image, as displayed by the Foresight™ ICE probe, three probes (A, B, and C) were tested. The ultrasound probe was held motionless in open-air using a clamp. Imaging contrast was set to ensure maximum brightness in the circular image and obtain a sharp boundary against the dark background (see figure 4). The size of the full image captured was 1920x1080 pixels. The imaging depth, also referred to as the field-of-view (FOV), was set to 80mm for the initial configuration. The imaging angle was swept manually between the minimum and maximum achievable values, thus acquiring the console image at 18 different angles. For probe A, these imaging data were acquired for each of the following FOV values: 75, 70, 65, 60, 55, 50, 45, 40, 30, 20, and 10mm. For probes, B and C, a less exhaustive dataset was acquired, at a FOV of 65mm and at 18 different imaging angle values.

From each ultrasound image, the radius of the circular image was computed using an automated approach to ensure consistency. The radius was defined in terms of the number of pixels. The relationship between ROI radius and imaging angle was determined by fitting a curve to the data. A similar approach was used for all data

collected for probes A, B, and C. A relationship was also established for normalized radial data points to provide a generic relationship in case a different image resolution is used.

Results: For probe A, the radius of the circular ROI was measured for 12 different imaging depths or FOVs. The results, as seen in Figure 6, indicate that the relationship between displayed ICE image radius and imaging angle remains the same regardless of the imaging depth or FOV settings. They also indicate a strong direct relationship between the imaging angle and the size of the ROI.

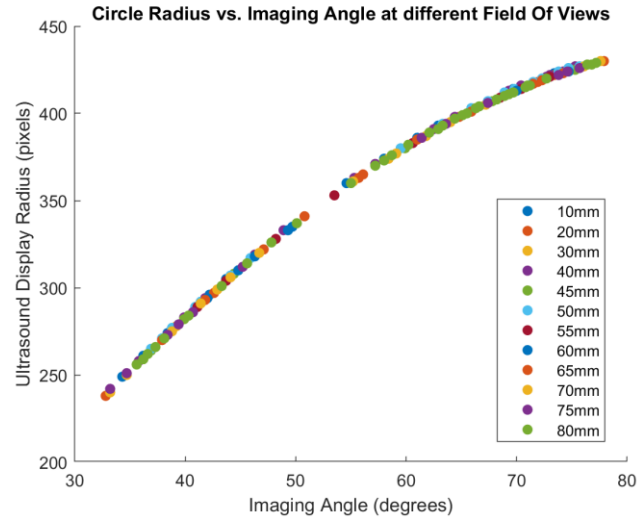


Figure 6 – Radius of the circular echo image displayed on the console vs. the imaging angle at which the ICE image is acquired. Each color represents a different imaging depth or FOV for which the imaging angles are swept from minimum to maximum.

For probes B and C, the imaging angles are swept at an imaging depth of 65mm. The radius observed at this FOV is shown in figure 7.

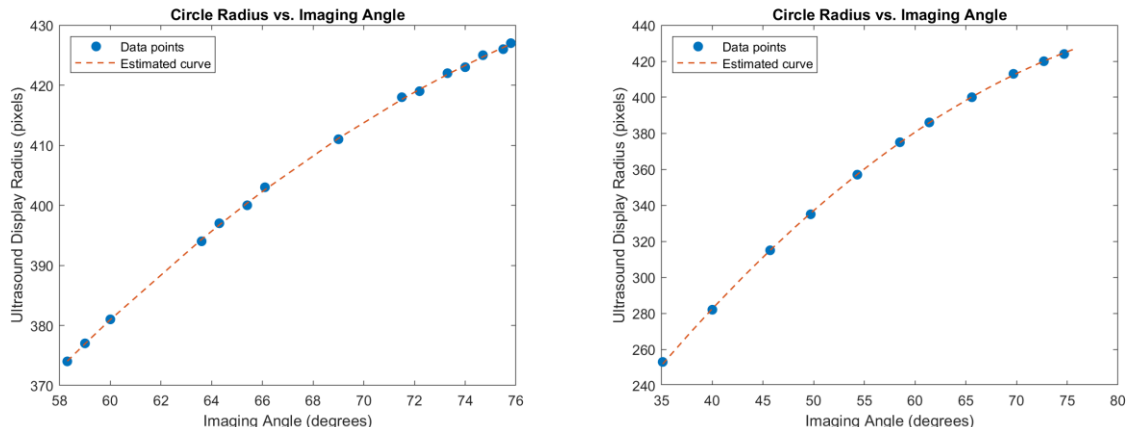


Figure 7 - Radius of the circular echo image displayed on the console vs. the imaging angle at which the ICE image is acquired for probe B (left) and probe C (right) at 65mm FOV. Data points are subsampled for display purpose only.

A second-degree polynomial was fitted to the individual datasets for each probe. Visual validation reveals that all three probes follow a similar trend (figure 8) with minor variability. The data from the three probes were combined to form a generic equation. Fitting a curve to this combined dataset produces a generic quadratic equation which can be used to calculate the radius of the ICE display given a certain value for imaging angle, at any FOV. The equation is given as:

$$\text{Radius (in pixels)} = -0.06\varphi^2 + 10.88\varphi - 56.92,$$

where φ represents imaging angle in degrees. It should be noted that the maximum imaging angle present in this dataset is 78 for which the radius becomes 430 pixels.

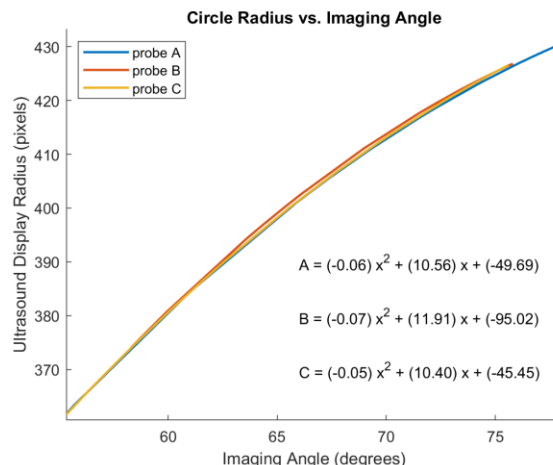


Figure 8 – Curve fitting to the absolute radius vs imaging angle dataset acquired at 65 mm FOV for probes A, B and C

For a more specific calculation tailored to a probe with a different maximum achievable angle, a normalized equation can be used. One manual measurement for the maximum radius value will be required in this case. Figure 9 shows the curve fitting to the normalized radius vs imaging angle combined-probe dataset. A more fitted equation to calculate the absolute radius of ICE is given as

$$\text{Radius (in pixels)} = (-0.14\varphi^2 + 25.31\varphi - 132.38) * 10^3 * (R_{max}),$$

where φ represents imaging angle in degrees and R_{max} represents the absolute radius value in pixels for the maximum imaging angle achievable by the chosen probe.

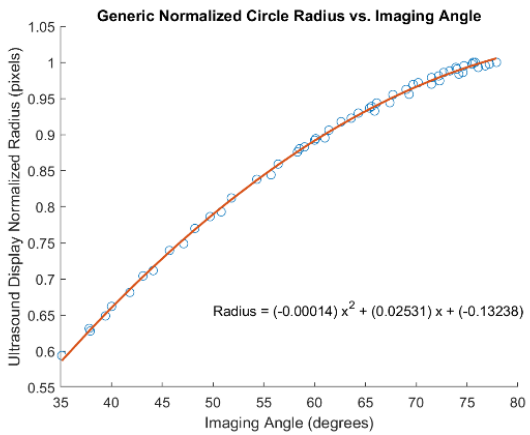


Figure 9 - Curve fitting to the normalized radius vs imaging angle dataset acquired at 65 mm FOV for probes A, B and C. Data points are subsampled for display purpose only.

Note: The curve is expected to become flatter at angles higher than 78. Some probes can achieve imaging angles up to 87 degrees, and if such a probe is used, it is recommended a few data points be taken to establish a closer fitting curve and a more accurate equation.

Conclusion: The curves for the three probes were similar but not the same. These differences might have been introduced by the potential discrepancy between the true angle and the displayed imaging angle of the ultrasound image.

In the above experiments, the size of the displayed ICE image is described in terms of the radius of the ROI i.e., the circular echo image displayed on the screen. From the results, we can conclude that:

- The size of the displayed ultrasound image is a function of the imaging angle.
- The radius of circular ROI varies positively and quadratically with the imaging angle.
- The radius of the ROI is independent of the FOV or imaging depth value chosen during imaging.
- The quadratic relationship between the radius of the ROI and imaging angle is fairly consistent between different probes as well.

First Scan-Line Consistency

Ultrasound probe tracking and calibration algorithms require that the ultrasound images are consistent with each other. For planar ultrasound imaging, this requirement includes that the first and last scan lines originate from the same transducer elements for each image acquired during the procedure. In the case of a single-element radial ultrasound, the first echo beam must be always generated from the same radial position. For the Foresight™ ICE probe, this translates to the angle of rotation (theta) of the first scan line being identical for each ultrasound image in its position in 3D space.

In this section, we evaluate the consistency among the radially acquired ultrasound images in terms of the angle of rotation (theta) for the Foresight™ ICE. The Foresight™ ICE probe has a sophisticated design with a single transducer element, supported by a vertical fulcrum, surrounded by a metal shield. The element undergoes two

primary motions – spinning and tilting, as described in section IG (figure 1). At a certain imaging angle, the 360-degree spinning motion forms the conical image. During ultrasound imaging, when the imaging is ‘paused’, the spinning motion comes to a halt. Because of the momentum, the element may initially stop at a different radial position than from where it started. The Foresight™ ICE probe has built-in functionality that further spins the transducer until it is positioned at the starting (first scan line) position. In this study, we observe how the first scan line may change both during an imaging session or study due to the pause feature, and between different studies.

Methods: To check the consistency of scan lines for a given ICE probe, we designed a simple and effective experimental configuration. An ICE probe was fixed in one position, submerged in a water bath. A needle was placed at a fixed position in the imaging field of view of the ICE to provide a fixed reference object, and the scanner parameters were set to an imaging depth of 80mm and an imaging angle of 70 degrees. Multiple sample images were acquired for different conditions and trials. Each image was cropped to acquire an ROI of size 850x850 pixels. From the first image, the automatically computed centroid of the needle reflection was used as a reference for a scan line. For each subsequent ultrasound image, the centroid was again computed using the same method. Given that the probe and the needle are fixed throughout the experiment, if there is no change in the angular position of the first scan line, then all the centroid points should coincide. The differences and offsets in the reference scan line were measured in terms of linear and angular displacement. The displacement measurements are described in terms of the number of pixels as well as in SI units i.e. millimeters. The pixel spacing was used to convert the number of pixel errors to real-world measurements, as calculated based on the following equation, where the radius was set to 80mm as set in the experiments.

$$\text{Radius (mm)} = \text{Pixel spacing (mm/pixel)} * \text{Number of pixels (pixel)}$$

$$80 \text{ mm} = \text{Pixel spacing} * 850/2 \text{ pixels}$$

$$\text{Pixel spacing} = 0.188 \text{ mm/pixel}$$

The scan line consistency was checked for the following conditions: use of the pause feature; beginning a new study; re-plugging the ICE probe in the PIM (Patient Interface Module) connector; and restarting the entire Conavi’s Hummingbird console. The following steps (Figure 10) were followed, and imaging samples were collected for this experiment.

Trial 1) Open a new study, **sample**, pause, **sample**, pause, **sample**, exit study.

Trial 2) Open a second study, **sample**, pause, **sample**, pause, **sample** exit study.

Trial 3) Open a third study, **sample**, pause, **sample**, pause, **sample** exit study.

Trial 4) Re-plug the probe into PIM, open a fourth study, **sample**, pause, **sample**, pause, **sample**, exit study.

Trial 5) Plug out the ICE probe, restart the console, plug in the probe, open a fifth study, **sample**, pause, **sample**, pause **sample**. exit study.

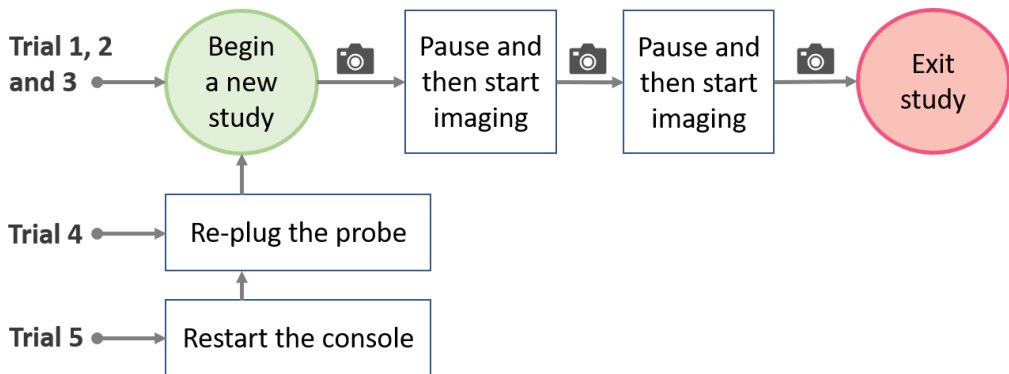


Figure 10 – Action steps for trials 1-5. The camera icon represents where the image was acquired.

Results: After obtaining centroids of the needle reflection from each of the ultrasound images, all the centroid points were displayed on a single image. Figure 11(left) shows all the centroids placed on the first image from the first trial. It can be seen that all the points do not overlap. A closer observation of the point distribution can be seen in figure 11(right), which shows that the points from trial 4 and trial 5 are significantly farther away from those collected from the other trials.

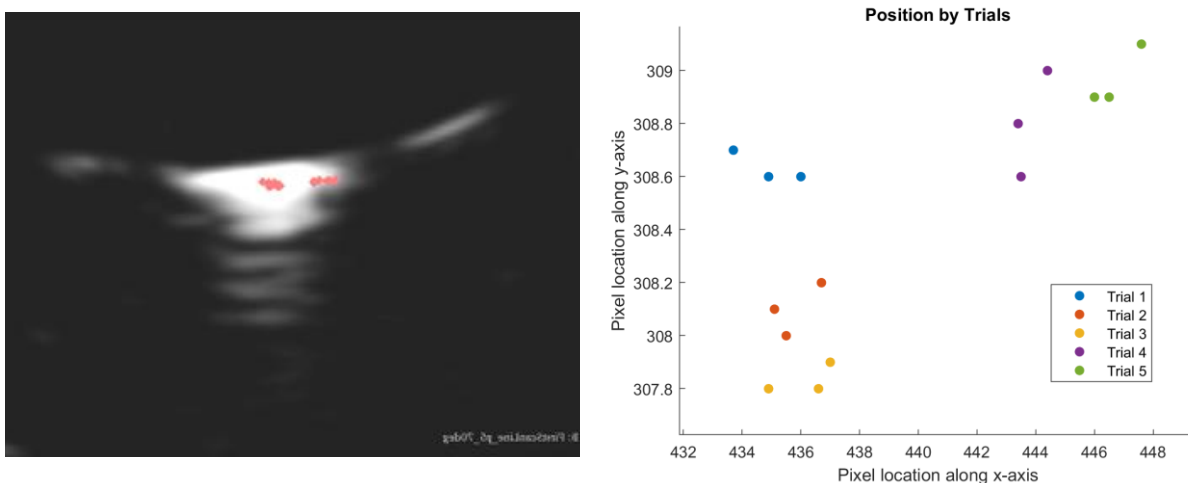


Figure 11 – (left) Reference image from Trial 1 overlaid by the centroids from all the trials.
(right) Looking closely at the spatial distribution of centroids obtained.

Relative linear and angular displacement was measured with respect to the centroid point from the first image of the first trial, as shown in figure 12. It should be noted that only the angular displacement is the measure of interest here since the variable parameter during radial scanning is the angle of rotation (theta).

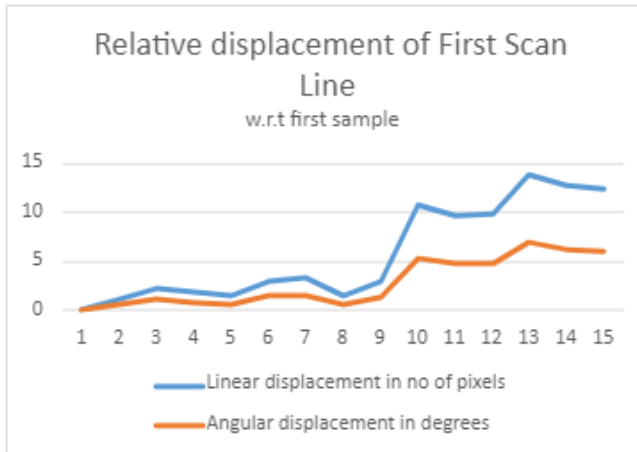


Figure 12 – Displacement of each sample point relative to the centroid from the first scan line of the first image of Trial 1 obtained.

When looking at the displacement with respect to the first image of the first trial, the maximum relative linear displacement was observed to be 14 pixels or 2.5mm. The maximum relative angular displacement was observed for trial 5 with a difference of almost 7 degrees.

Within each trial, we measured the displacement of each sample point relative to the first sample of that trial. On average, the linear displacement within trials is almost 1 pixel (1.2 pixels) or 0.2mm. The angular displacement incurred through the use of the “Pause” function is 0.6 degrees on average which is negligible. Some of the errors in this experiment can also be attributed to the systematic fiducial localization error introduced by the large size of a needle reflection.

Conclusion: Looking at the spatial distribution of points, changes between trials, and relative changes within each trial, we can conclude that:

- The first scan line remains similar as long as the probe is plugged in.
- Pausing the imaging during a study does not lead to any significant changes in the angular position of the first scan line.
- Starting a new study, without plugging out the probe, also does not cause any significant change in the angular position of the first scan line.
- The first scan line for a probe will change its angular position once the probe is re-plugged or the system is rebooted.

Based on the results and conclusions derived from it, we can infer the following guidelines when operating the Foresight™ ICE probe.

- In a clinical setup, where the probe is plugged only once and is not re-used, the first scan line remains consistent. This means that no additional measures for probe calibration and tracking are required in a real clinical scenario with one-time use of the ICE probe.

In an R&D setup, where one probe is potentially reused for multiple experiments, the first scan line may not be the same each time. This implies that the probe should either be recalibrated or the calibration to be manually adjusted each time it is plugged in for a study.

Imaging Angle Consistency

The imaging angle or tilt angle ‘phi’, displayed on the screen is a major factor in image reconstruction and 3D image processing, since inaccuracies in this measurement will result in faulty 3D image reconstruction. The angle is determined by the sensors embedded within the ICE catheter. While the user can control the imaging angle manually, nevertheless some unintentional changes were observed in this parameter. The trueness, accuracy, and behavior of the imaging angle may depend on some internal or external factors to the ICE probe.

Internal factor – Angle trueness: The accuracy of the imaging angle is said to be in the range of ± 5 degrees., as reported by the manufacturer. Studies were conducted in our lab to characterize the inaccuracy in imaging angle however the results were inconclusive due to the hypersensitivity of the imaging resolution. Our setup required target localization in the image and even a difference of one pixel in localization would change the predicted imaging angle by one degree.

It should be noted that while a 10-degree offset can cause inaccuracies in a 3D guidance system, this error is unlikely to cause any adverse effects during the intended use of the ICE probe in intraoperative ultrasound imaging situations.

External factor – Gravity: The imaging angle of the conical ICE image also changes with respect to the physical orientation of the probe. For example, if the probe is horizontally positioned and the imaging angle is 75 degrees, then the angle can decrease by as much as 6 degrees (to 69 deg) when the probe is held vertically. This change in angle is also captured by the angle sensor and reported on the console display. Therefore, this change in angle will neither cause a discrepancy in intraoperative imaging nor in an image guidance system.

Image Artifacts

Foresight ICE probe is a radial ultrasound imaging technology and can experience all the same imaging artifacts as a planar ultrasound, such as acoustic shadowing, enhancement, reverberations, etc. Apart from the common imaging artifacts, we have observed three atypical effects namely: donut, ring, and sprinkler artifact.

Donut artifact: The Foresight ICE probes have an inherent hollow circular region, either completely bright or dark, in the center of the image at the apex of the cone. This absolute ‘black-out’ or ‘white-out’ zone in the middle is inherent to each catheter. Imaging is not possible in this region. The width of this region is predefined to be at least 5mm. In the DICOM files, these pixel locations store some of the header information. Figure 13 shows an example of a white-out donut artifact.

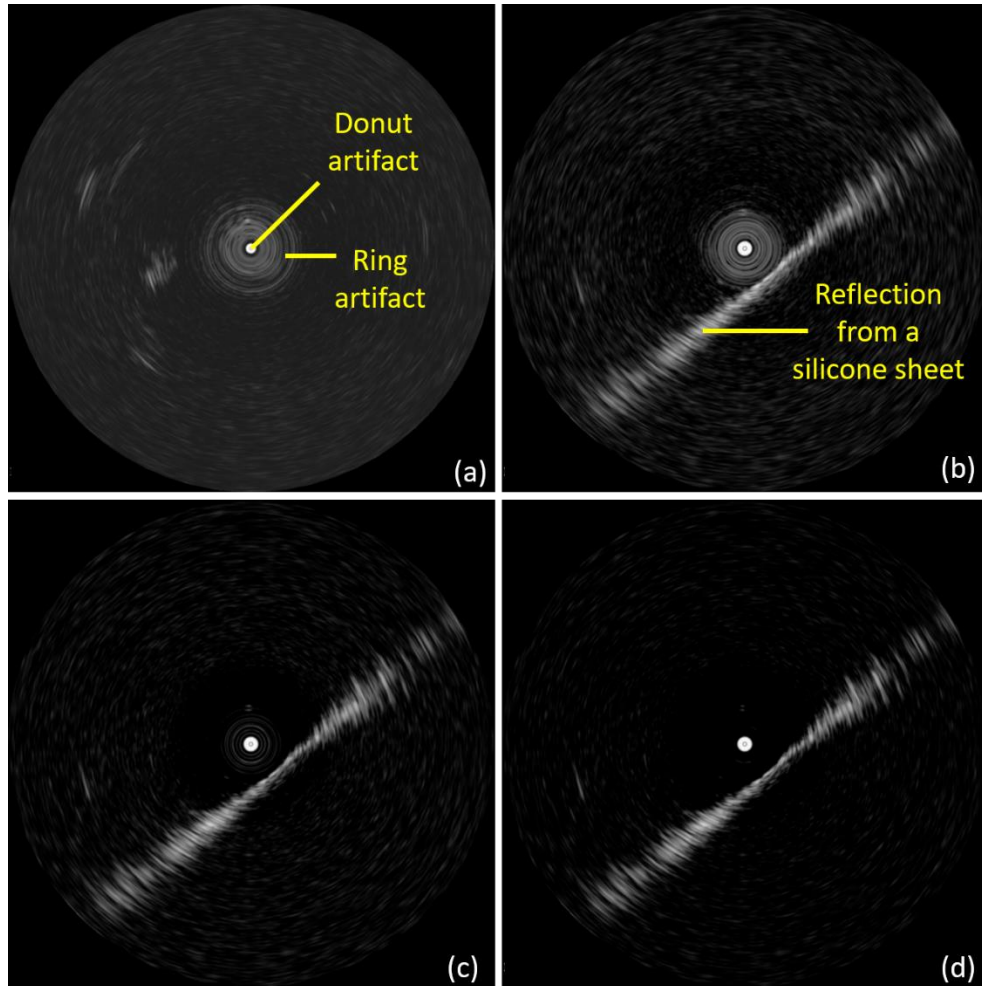


Figure 13 – ICE imaging in water bath showing (a) central white-out donut artifact and ring artifact, (b) ring artifact overlaying a reflection from a silicone sheet. Ring artifact is minimized by using the ‘magic-wand’ button a (c) medium and (d) highest setting.

Ring artifact: The central hollow region is surrounded by a series of bright, concentric rings that can occupy up to a few millimeters of radial space in the ICE image. This ring artifact is a result of near-field noise present in the catheter. It is unique to each ICE probe and may change between multiple uses of a single probe. The appearance of the rings is overlaid on top of the echo image and ultrasound reflections can be seen within the region of the ring artifact. It is worth noting that the rings are constant during a study and do not present any motion or changes in brightness. Thus, the operator’s eyes, when focused on ultrasound imaging, can easily accommodate the presence of these rings. However, these artifacts do present a challenge in the design of image

processing techniques. Nevertheless, the appearance of the rings can be minimized by manually adjusting the windows and level functionality or using the automated “magic-wand” function included in Conavi’s Hummingbird console (see figure 13(b-d)).

Sprinkler artifact: The Foresight™ ICE probe was used in a tracking environment as well. In a table-top tracking system (Aurora, NDI), there is an ellipsoidal volume of low-intensity varying electromagnetic field. In the presence of varying electromagnetic field, interference was observed in the ICE imaging causing a sprinkler effect (figure 14). This artifact includes a series of bright speckles in a curved line along with the radial depth of the ICE image. The speckles rotate with the spinning of the transducer. The intensity of the bright speckles decreases as the probe is moved farther away from the tracking system. The artifact can be seen in the images whether the ICE probe is equipped with an EM tracking sensor. Similar to the ring artifact, these bright speckles can cause an issue in the design of an image-guided system that relies on magnetic tracking of the probe, and which involves processing the ultrasound image captured directly from the screen.

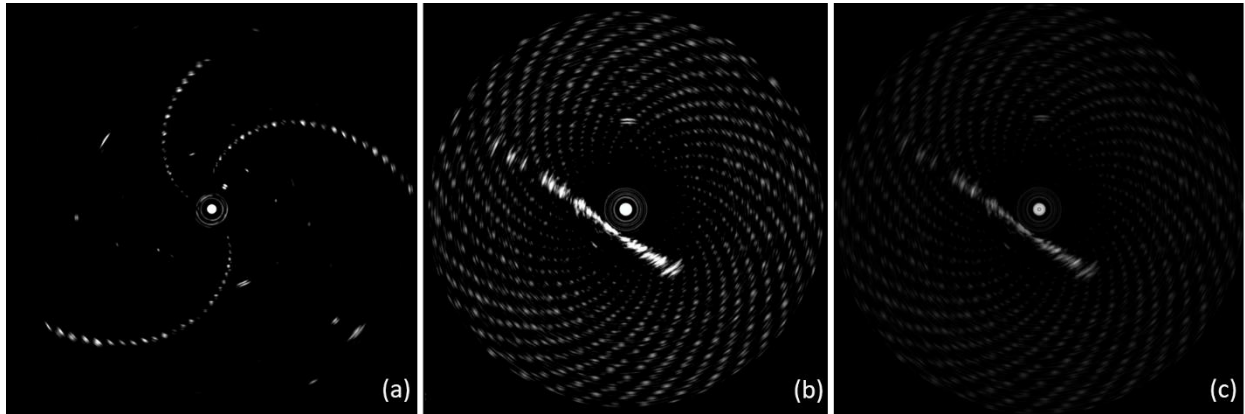


Figure 14 – (a) Sprinkler artifact seen as a foreground. (b) Sprinkler artifact variation (enhanced) seen in the background and (c) brightness adjusted to minimize the background sprinkler effect.

II. ICE Image Visualization (Slicer-compatible)

Volume Reconstruction & Rendering

The ICE image is visualized on the console monitor screen as a 2D circular image. To visualize the true, conical ultrasound image lying in 3D space the circular image must first be converted into 3D volume form, followed by processing with a volume rendering technique. All processing and off-line visualization was performed within the 3D Slicer. We implemented a Slicer module called ‘ICE Reconstruction’ which implements the 3D reconstruction of the 2D ultrasound image, as well as the rendering of foreground of the volumetric image. The module implements the mathematical reconstruction described in the section IDA. The slicer-compatible python function for the reconstruction of ICE image is added in appendix A. The module utilizes the existing ‘Volume Rendering’ module to render the 3D conical ICE image. Since this visualization technique is composed of voxel information, the volume rendering shows the foreground echo information while blanking out the background / dark regions from the ICE volume. Figure 15 shows a sample ICE image and its volumetric reconstruction and rendering via the designed Slicer module. On an average computer, the volume reconstruction takes almost 100ms of time.

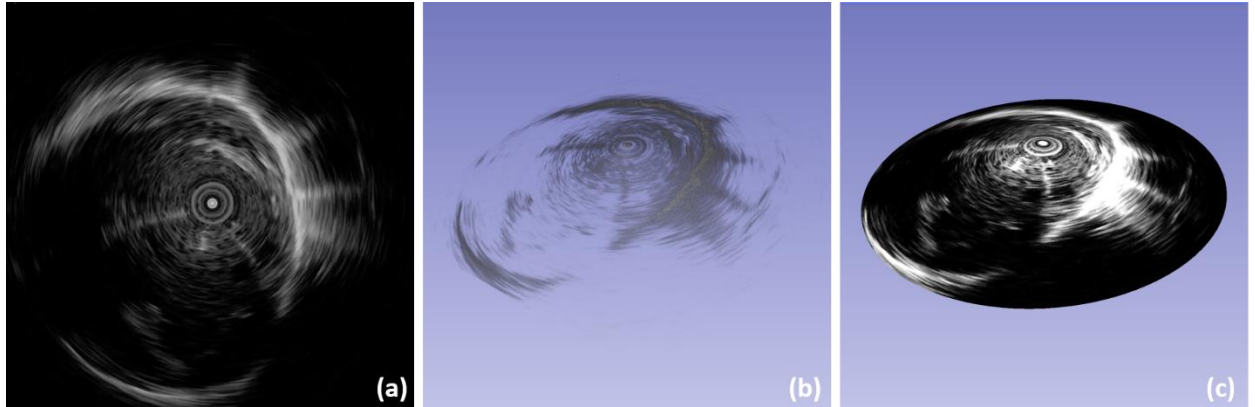


Figure 15 – (a) ICE image as seen on the console, (b) after volume reconstruction and rendering in 3D space, and (c) after texture mapping to a cone model via Slicer module.

Surface Texture mapping

Another way to visualize the 3D conical image is to texture map an image on to the surface of a cone, which is implemented in 3D Slicer using the available VTK (Visualization Toolkit) methods. VTK is an open-source platform for observing and handling scientific data. In texture mapping technique, an image (as a texture) is mapped on to a surface model. In this case, the ultrasound image, cropped to focus on the ROI, serves as the texture image. Thus the image is set as an input to the function `vtkTexture`. Then to create a surface model, a cone shaped model (`vtkConeSource`) acts as a planar surface. Finally, the `vtkTextureMapToPlane` method is used to map the textured image on to the cone, where the cone source is set as the input connection or the “plane”. For accurate mapping, the textured image coordinates need to align with the geometry of the cone according to figure 16. The center of the cone, which lies midway on the major axis of the cone connecting the

apex to the base of the cone, should align with the center of the image. The texture mapped cone is now ready to be rendered in any 3D visualization software. To view this cone in 3D Slicer, the cone source is rendered as a model and can be manipulated or compounded with spatial transforms. An example image and its texture mapped visualization can be seen in figure 15(c).

On an average computer, texture mapping can take up to 17ms, which is adequate for real time visualization and data streaming. A Slicer-compatible python function for texture mapping an ICE image, given an imaging angle, is included in appendix A. A complete module is also available at this link: TBD.

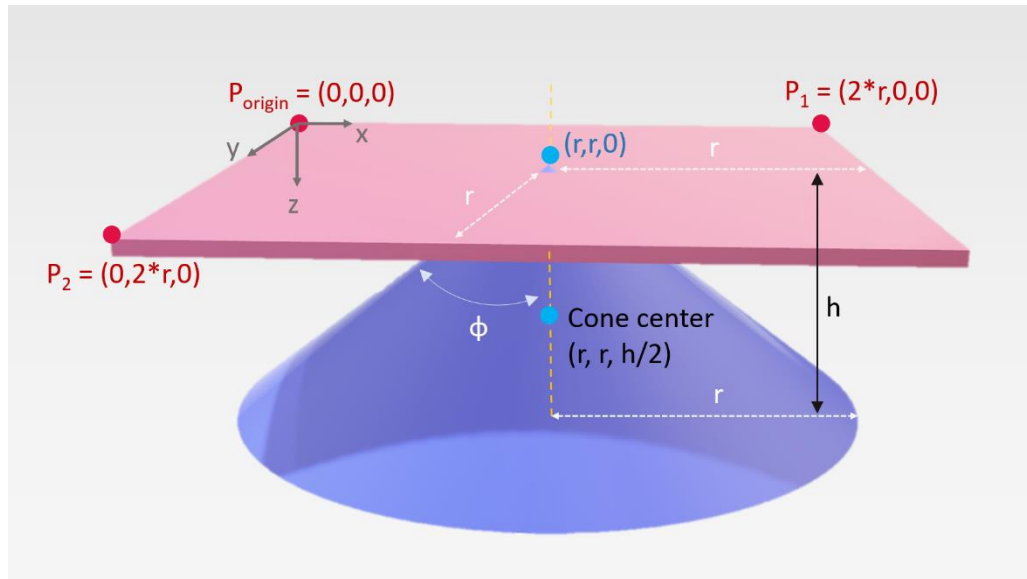


Figure 16 – Schematics of texture mapping of ICE image to a cone model

DICOM reconstruction and custom interpolation

The Foresight ICE probe has a single element transducer and acquires the ultrasound data radially. As such, when the ultrasound is stored as a DICOM file, there is an obvious change in geometry and the appearance of image in an image-viewing software. Figure 17 shows how each radial echo beam is stored as one complete row in the DICOM file. As the element spins the angle of rotation increases, and the subsequent echo beams are stored as the next rows.

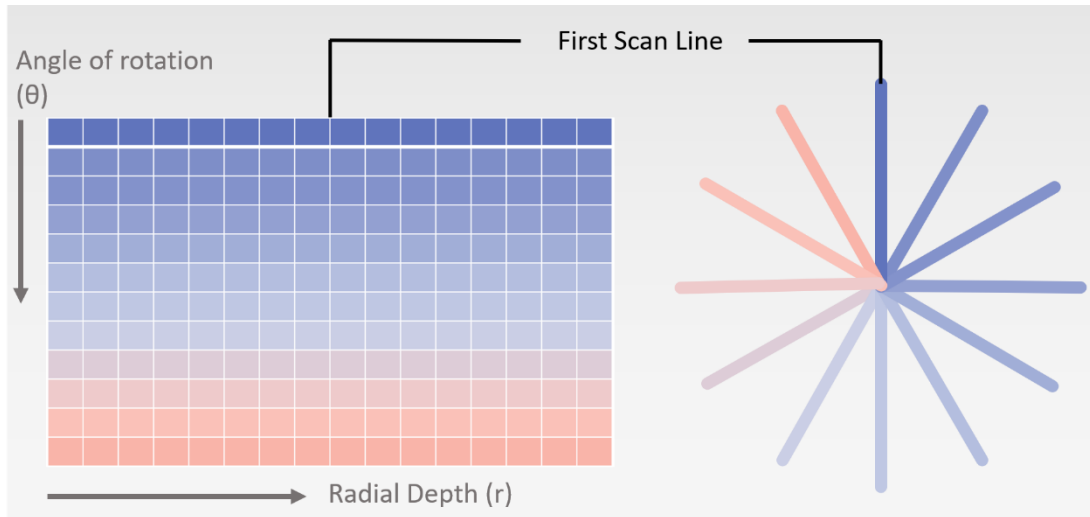


Figure 17 – Schematics of storing radial and spinning ultrasound beams (right) acquired via Foresight ICE probe as DICOM file (left)

The first few pixels in any row, representing the donut-artifact area near the apex of the conical image, are overwritten with supplementary header information, while the rest contain the true echogenic information. Some of the important header information to reconstruct a conical image and their respective DICOM access code are given below:

- 1) A value for imaging angle (phi) – [0x15, 0x1000]
- 2) A value of angle of rotation for each row or echo beam – [0x15, 0x1004]
- 3) Spacing information along the radius. – [0x28, 0x0030]

The value for imaging angle (phi) is already available in degrees. The values for rotational angle (theta) however are encoded and must be converted to degrees using equation:

$$\text{Theta (in degrees)} = \text{Theta (encoded)} / 1024 * 360$$

In order to reconstruct the 2.5D conical image, we find the cartesian coordinate location of each pixels using the information above i.e., radial echo sample, radial spacing, theta and phi. The complete code for reconstruction is added in appendix A.

It should be kept in mind that each ultrasound frame, consisting of one spinning motion, contains roughly 350 radial beams. When the DICOM file for one frame is reconstructed, the radial beams are sparse, lying far apart in 3D space as can be seen in figure 18(a). In the appended code we add an additional function to interpolate the image. The interpolation is performed on the DICOM file before the reconstruction. The user chooses the degree of interpolation and rows are added between existing row image-data accordingly. The improvement in visualization upon interpolation can be seen in figure 18(b, c).

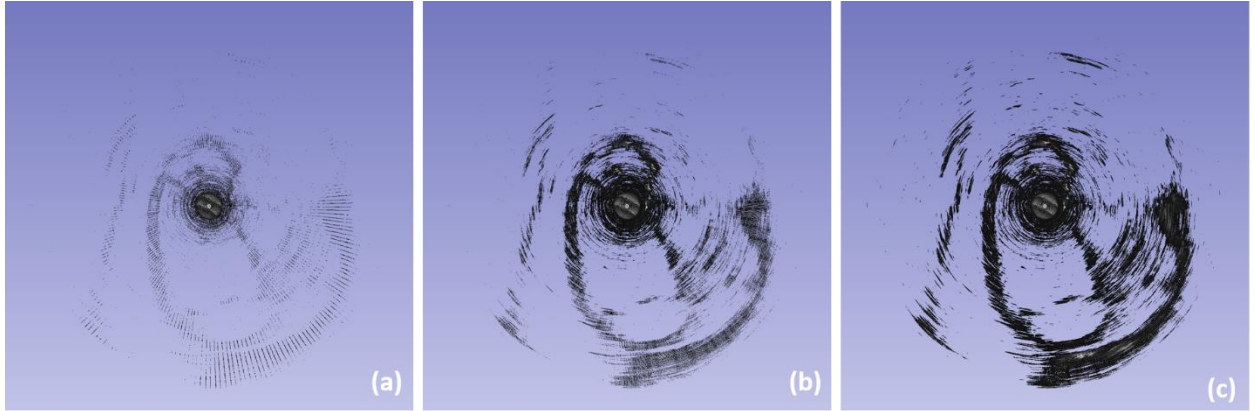


Figure 18 – (a) Conical ultrasound image reconstructed from the dicom file and with interpolation factor of (b) 5 and (c) 15.

III. ICE Probe Calibration

Temporal calibration

In an electromagnetic tracking environment, and our data acquisition system, there are many different systems and machines at hand such as the PLUS server connection, the tracking system, the ultrasound machine, and the PC software recording the data (3D Slicer). It becomes important to know the time delay between these systems in designing an image guided system. Temporal calibration is performed to find the latency between the ultrasound generated image and the corresponding tracking signal.

Method:

We use a temporal calibration method described by Gobbi et al. and extend it to work for the 2.5D images. This approach compares the positions of a tracked, line-shaped object in real space to those of the reflection of that object as seen in a B-mode ultrasound images. We use a 4 mm wooden shaft to represent a line and its reflection is seen as a point in the ultrasound image. Wood is used to reduce the amplitude of the reflection at the shaft-water interface. The line is kept almost perpendicular to the 2.5D imaging plane to obtain a bright and well-defined reflection in the ultrasound image. A 6 DoF magnetic tracking sensor is rigidly attached to the shaft representing the line to track its motion. Accuracy of this method is highly dependent on the linear motion of the line with respect to the ultrasound image. To ensure smooth and unidirectional motion of the line-object, we fashioned a simple, plastic building-block assembly which moved along the tracks at the bottom of the water bath. The Foresight ICE probe remained static at one position. The block assembly carrying the wooden line-object is moved forward and backward along the tracks to generate a sinusoidal motion pattern. Reflections in the image appear in and out of the imaging angle accordingly. Five measurements were taken with imaging angle fixed at 85°. For every measurement, at least 2 motion cycles were recorded.

Segmentation of the line reflection from the images was performed automatically using 3D Slicer. The centroid of each segmented reflection from the images was extended to 3D space using Eqn. 1. The distance of this point from the origin O of the conical image is recorded to represent the positional information of the object in the

image (img_{dist}). To obtain the positional information of the line-object in real space (obj_{pos}), the tracking sensor data were analyzed to find the linear direction of motion using Principal Component Analysis and record the projection of sensor position along the principal axis. The two signals representing position of the object in space (obj_{pos}) and its reflection in the image (img_{dist}) were normalized by subtracting the mean followed by division by the standard deviation in a signal. Finally, the temporal offset was calculated by finding the time delay which provides the highest cross-correlation between the two signals. We repeat our temporal calibration experiment at multiple imaging angles to evaluate the precision of the calibration. The experiment was repeated multiple times at three different imaging angles, keeping the probe still and only changing the imaging angle through the console.

Results:

The tracked long wooden line was moved in and out of the conical 2.5D surface plane of the Foresight ICE probe fixed at an angle of 85° . Correlation was used to find a temporal offset between the two sinusoidal signals: position of line in 3D space (obj_{pos}) and distance of point reflection from the center of the image (img_{dist}). A time delay of 72 ms was observed in this experiment. Figure 19 shows the normalized signals before and after temporal calibration.

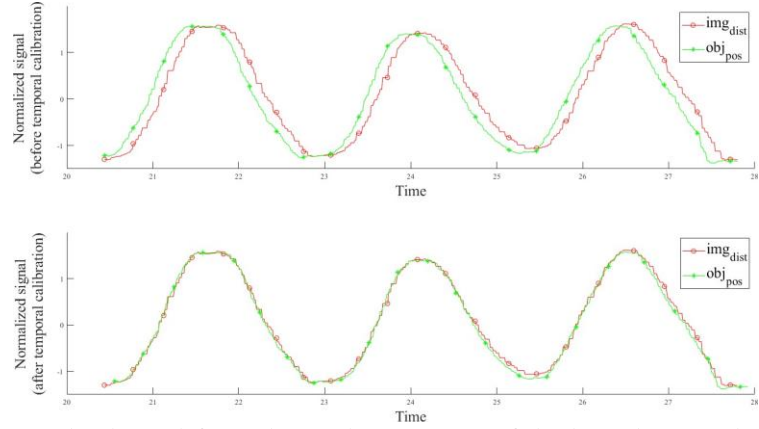


Figure 19 – Normalized signals, derived from the tracker position of the line-object and its reflection in the ultrasound image, before and after temporal calibration is applied.

The experiment was repeated at 3 different angles with at least 5 measurements at each angle. Every measurement includes a minimum of two sinusoidal motion cycles. Results are summarized in Table 1.

ϕ	Mean temporal offset (ms)	Standard deviation (ms)
85°	98.6	± 12.8
75°	86.7	± 16.9
65°	93.7	± 21.6

Table 1: Precision of temporal calibrations performed multiple times at different imaging angles

An overall mean temporal offset of 93ms was observed. While a 93ms offset may account for an appreciable portion of a patient's cardiac cycle (particularly at higher heart rates), this time delay does not make a perceptible difference in a clinical setting for most applications such as ablation therapies and visualization. However, for

some applications involving rigorously moving structures, such as segmentation of mitral valve leaflets, this time offset may cause errors. Therefore, for general purposes it is not crucial to correct for temporal offset, but some interventions might require it to achieve higher accuracy.

Spatial calibration

Ultrasound-based image guidance systems typically employ tracked tools and a tracked imaging probe. The use of electromagnetic tracking with ultrasound imaging facilitates the registration between patient anatomy, ultrasound images and other imaging modalities such as preoperative CT and MRI, and even electrophysiology maps to guide atrial ablation procedures. Tracking is achieved using position and orientation (pose) sensors attached to the imaging probe. The tracking system generates a transformation between the sensor attached to an ultrasound device and the reference/world coordinate system, but the pose of the ultrasound image with respect to this reference coordinate system is unknown. Therefore, ultrasound calibration is required to determine the transformation between the coordinate system of the image volume and the sensor attached to the probe. We present a method for the spatial calibration of the Foresight™ ICE probe which possess a unique 2.5D conical imaging.

Methods:

In all our experiments, tracking is achieved using an electromagnetic tracking system (Aurora, NDI, Canada). The Conavi Hummingbird console along with a Foresight ICE probe is used to generate ultrasound images. We formulate ultrasound probe calibration as a registration problem between a point and homologous line, using a tracked needle (a line) and its hyperechoic reflection in ultrasound image (a point) as the basis for calibration. While the Foresight ICE generates a conical ultrasound image in real time, it is displayed on a conventional 2D monitor as a disc-shaped image in a 2D polar coordinate system. Given the imaging depth r and the imaging angle φ , the 2D pixel location in the original disc image can be converted to a 3D coordinate system as per Eqn.1. In this manner, the point-line based calibration is directly applicable to the Foresight ICE probe calibration, where efficient solutions exist.

A Foresight ICE probe was augmented with a 6 DoF magnetic tracking sensor rigidly attached to the outer sheath, close to the probe tip. A water bath was scanned at room temperature using tracked a Foresight ICE probe. A pre-calibrated needle (Aurora Needle, 18 G/150 mm, NDI, Canada)¹¹ was used to model a line. The pose of the needle is defined by a point of origin and a direction vector. The needle was oriented at multiple positions and angles to produce point fiducials on the cone shaped 2.5D images, along the radius and at varying azimuthal angles θ . For this initial assessment, the imaging angle φ was kept constant at 80°. Clamps were used to minimize jitter and overcome inaccuracies caused by temporal misalignment. 15 point fiducials were recorded using screen-capture of the Conavi console, along with the tracking information for both the probe and the needle. Fiducial points from the 2D images were converted using Eqn. 1 to their correct representation in 3D space.

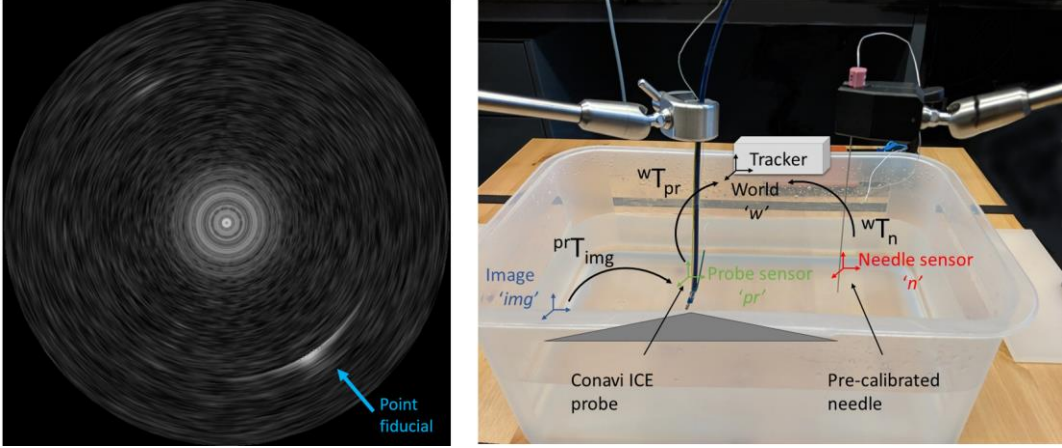


Figure 20 – (a) Screen capture of Foresight ICE image as seen on the Hummingbird console and (b) experimental set up for data acquisition. Arrow shows the reflection of the needle as seen in the ultrasound image

The coordinate systems are represented in Fig. 20(right), with that defined by the magnetic tracking system being considered as the world coordinate system. Let w , n , pr and img represent coordinate systems as defined by the tracker, needle sensor, ICE probe sensor and ultrasound image volume, respectively. As the needle is pre-calibrated, the transform P_1 from needle tip to the sensor on the needle is known. The pose of the line fiducials can be defined in coordinate system of the ultrasound probe using:

$$P_2 = {}^{pr}T_{img} = ({}^wT_{pr})^{-1}({}^wT_n)P_1 \quad (2)$$

where ${}^wT_{pr}$ and wT_n are the locations of the probe sensor and needle respectively, as reported by the magnetic tracking system. Fiducial point coordinates in 3D space and pose information of the line fiducials (P_2) are used to solve for the affine calibration transformation comprising of anisotropic scaling, followed by rotation and translation.

Validation

We validated our calibration both qualitatively and quantitatively. Qualitative assessment was performed by generating a model of the needle used for spatial calibration and displaying its intersection with the 2.5D ultrasound image in a virtual reality environment. We also validated our calibration system by evaluating the precision of spatial calibration parameters. To validate the overall system accuracy, two experiments were performed: point source localization and calculation of the centroid of a spherical object. We designed a phantom which can be used to model both the point source and a sphere object and compare the point and centroid location with pre-experiment reference positions defined by the CT scan of the phantom.

Calibration Precision

Conventionally calibration precision is evaluated at multiple depths and frequencies. Variability of parameters, as calibration is performed at different depths and frequencies, is extensively discussed in literature. Since Foresight ICE has the functionality of adjustable imaging angle φ of the cone shaped image, we intended to

observe the trends in variability, if any. We repeat our spatial calibration experiment at multiple imaging angles to evaluate the precision of spatial calibration matrix parameters: translation along Cartesian axes, Euler rotation angles and scaling along Cartesian axes. In all the experiments the probe was physically held in place using a clamp and the imaging angle φ was changed through the buttons on the console. Automatic segmentation was performed using 3D Slicer to locate the needle point fiducial in the 2D images. The remainder of the procedure was as described in the methods above.

Point Source Localization

A 140 mm by 140 mm plate phantom was designed with 4 pillars in each corner, one in the middle and 7 divots. The divots help define the reference coordinate frame via point-point registration of divot locations from tracker coordinate system to CT coordinate system. The corner pillars secure the wires going across and intersecting at one point, which is considered as the target point source (Fig. 21(a)). The wires were roughened near the intersection to improve their echogenicity. The cross-wire phantom was scanned using the calibrated Foresight ICE probe to image the point source. A 5 mm thick layer of silicone was poured into the bottom of the phantom to help reduce reflections. Care was taken to position the probe such that the point fiducial lies in the middle of the cone shaped image along the radius, in order to minimize the beam profile effect and associated errors. Points are converted to 3D space using Eqn. 1 followed by calibration transformation and conversion to reference coordinate system defined by the CT scanner. The ground truth is established by the point location in the 3D CT scan. Point reconstruction accuracy is described in terms of standard error and 95% confidence interval along x, y and z axis.

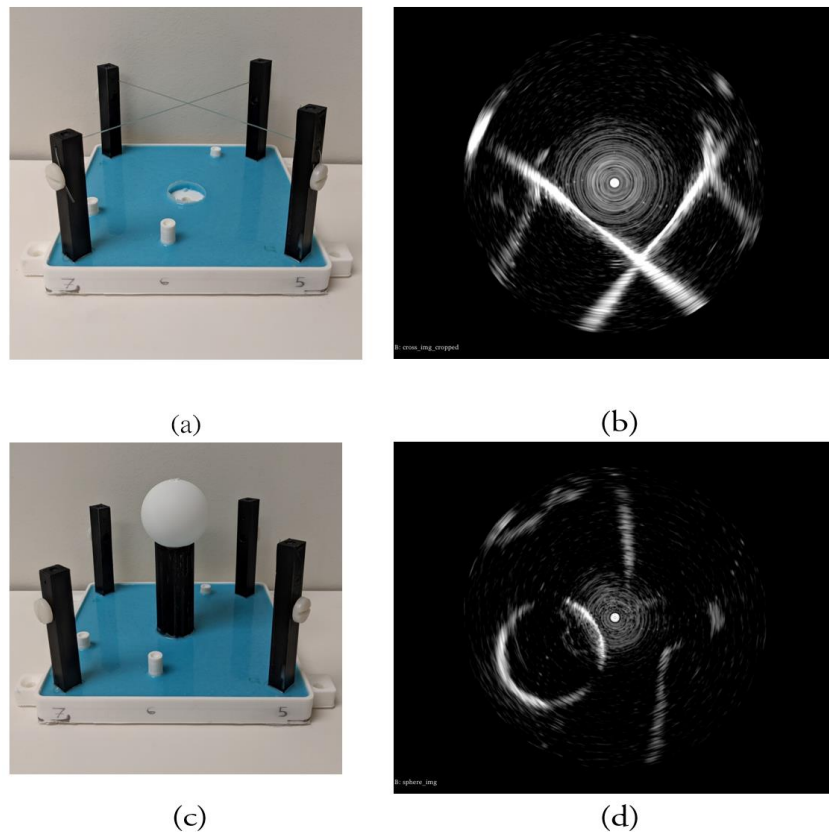


Figure 21 – Validation phantom: (a) cross wire to model a point source, (b) as seen in 2.5D ultrasound and (c) sphere ball, (d) as seen in 2.5D ultrasound.

Spherical Phantom Centroid

The same phantom was adjusted to remove wires and add a 30 mm radius table-tennis ball to model a sphere. The phantom was imaged at multiple poses to identify points along the outline of the sphere at different cross-sections (Fig. 21). Then, similar to the point source localization method, the points were transformed to the reference coordinate system. Spherical fitting was applied to these points to find the center and radius of the sphere. These centroids of the sphere were compared to the one estimated in the reference coordinate system.

Results:

Spatial calibration of a fixed-angle Foresight ICE probe, with a magnetic sensor attached to the outer sheath, was performed using a needle phantom and point to line registration algorithm. Results depict an overall calibration accuracy (fiducial registration error, or FRE) of 1.74mm.

Qualitative validation:

For initial validation, a qualitative assessment was performed. The 2.5D images were reconstructed from the 2D images obtained from the screen capture of the Conavi console. Transformations were applied to a virtual needle model and the reconstructed volume. Figure 22 shows the needle passing through the needle reflection or point fiducial seen in the image, providing preliminary validation of the calibration method.

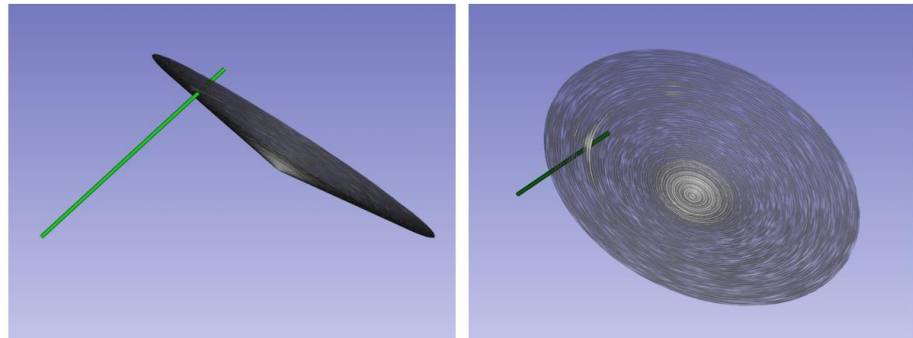


Figure 22 – Qualitative validation of calibration method in virtual space. Needle passing through the reconstructed 2.5D ICE image: (a) side view, and (b) top view.

Calibration Precision:

Spatial calibration of Foresight ICE probe with a unique 2.5D image was repeated at 5 different angles to observe the translation, rotation, and scaling factors of the calibration. Table 2 shows the precision of different parameters of spatial calibration.

ϕ	t_x	t_y (mm)	t_z	r_x	r_y (°)	r_z	s_x	s_y (mm/pixel)	s_z
85°	-2.68	-1.02	6.22	-0.20	-0.01	2.56	0.16	0.16	0.59
80°	-2.85	0.18	8.87	-0.34	0.28	2.56	0.16	0.17	0.16
75°	-2.26	-1.00	0.54	-0.30	-0.12	2.36	0.16	0.15	0.30
70°	-0.74	-0.51	9.92	-0.28	-0.19	2.43	0.15	0.14	0.25
65°	-4.77	0.19	8.33	-0.03	-0.29	2.35	0.17	0.17	0.11
Mean	-2.66	-0.43	6.78	-0.23	-0.07	2.45	0.16	0.16	0.28
RMS	1.29	0.54	3.34	0.11	0.20	0.09	0.01	0.01	0.17
$\pm 95\%$	± 1.13	± 0.47	± 2.93	± 0.09	± 0.17	± 0.08	± 0.01	± 0.01	± 0.15

Table 2: Precision of spatial calibrations performed at different imaging angles. The overall mean, root mean square (rms) error and 95% confidence interval is given for estimated spatial calibration parameters: translations (t_x , t_y , t_z), Euler rotations (r_x , r_y , r_z) and scaling factors (s_x , s_y , s_z)

We observe high variations along z-axis with root-mean-square error in translation (t_z) going as high as 3.3mm. This behavior was expected for two reasons. First, the imaging angle ϕ changes along the z-axis and there may be up to 5° of uncertainty between the imaging angle displayed on the screen and the true physical angle of the conical image in 3D space. Second, the calibration is performed using 3D reconstruction of the 2D screen-capture of the ultrasound image based on the imaging angle ϕ . This reconstruction is prone to some error because of possible data loss from projecting a 2.5D image to a 2D console screen and then reconstruction back to 3D space.

Point Source Localization:

The cross-wire phantom was secured firmly in a water bath and imaged using a freehand technique. The intersection of the wires, considered as a point source, was imaged from all 4 crossing angles to have a better estimate and reduce bias. B-scan images of the point source are acquired at 15 different positions. Points were manually segmented and converted to the reference coordinate system defined by the CT image volume. All the points were compared to the ground truth defined by the CT of the phantom. Standard error and 95% confidence limit for point reconstruction accuracy is given in Table 3.

Spherical Phantom Centroid:

The spherical phantom was scanned freehand from different sides. 20 images were acquired and almost ten points along the outline of the sphere were identified in each image. These points were randomly rearranged into 30 groups to enable unbiased distribution of points along the surface of sphere in each measurement. After reconstruction to 3D space, sphere-fitting and coordinate system conversion, the centroids were computed from each group of points and compared to the centroid defined by the CT coordinate system. Using the points on the surface of the sphere, we can also compute accuracy for radial distance and volume measurement, however they were deemed unreliable due to low ultrasound image quality. Table 3 summarizes the results for locating a sphere centroid in a 2.5D ultrasound image.

Validation method	Mean error (mm)			95% Confidence interval (mm)		
	x	y	z	x	y	z
Point source localization	5.07	5.0	4.2	± 2.62	± 2.58	± 2.16
Sphere centroid localization	1.75	0.91	1.94	± 0.64	± 0.343	± 0.7

Table 3: Accuracy of calibrated and tracked Foresight ICE probe described in terms of mean standard error and 95% confidence limits for point source localization and sphere location estimation.

Discussion

In this work, a calibration method for the unique 2.5D cone-geometry images acquired using a single-element, mechanically scanning intracardiac ultrasound probe was presented and evaluated. Qualitative analysis in a virtual environment shows that the needle intersects with the point fiducial in the 2.5D conical images after calibration. The FRE of the calibration was 1.74 mm in the initial study. However FRE alone does not accurately depict the overall efficacy of a tracking and calibration system. We quantify both the calibration methods and our overall tracking system. We perform point source localization to compute the target registration error (TRE) of the system. Results indicate mean standard error up to 5.07 mm. The 2.5D ultrasound images generated by a single-element mechanically scanning probe is a relatively new concept, and calibration accuracy may be improved once the image generation, acquisition and processing are better understood. Attaching a sensor on the outer sheath of the ultrasound probe also introduces errors in this tracking system. Ideally, the sensor will be integrated rigidly inside the probe, close to the transducer and does not cause any magnetic interference. We looked further into the reason why the TRE is so high, and the major cause is discussed in detail below.

Challenges

One of the biggest challenges faced when working with the tracked ICE probe, is the motion of the transducer element relative to the body of the ICE catheter. It was observed that the calibration and tracking were accurate when the probe is held stationary, however, any linear or rotational movement of the catheter introduced exceptionally high errors in the system. Once the probe is moved following calibration, the tracking becomes inaccurate due to a rotational angular offset. This offset is caused by the relative motion between the innermost part of the catheter with the transducer and the external sheath of the ICE probe where the sensor is attached. Figure 23 demonstrates this challenge visually. The left image represents the state of imaging and tracking immediately after probe calibration when the ICE catheter is not moved. The virtual needle can be seen intersecting the needle reflection in the ultrasound image. The right image shows the ultrasound imaging after the probe is moved. The error can be seen as the needle reflection follows the virtual needle at a rotational offset. This rotational offset was observed to be up to 60 degrees.

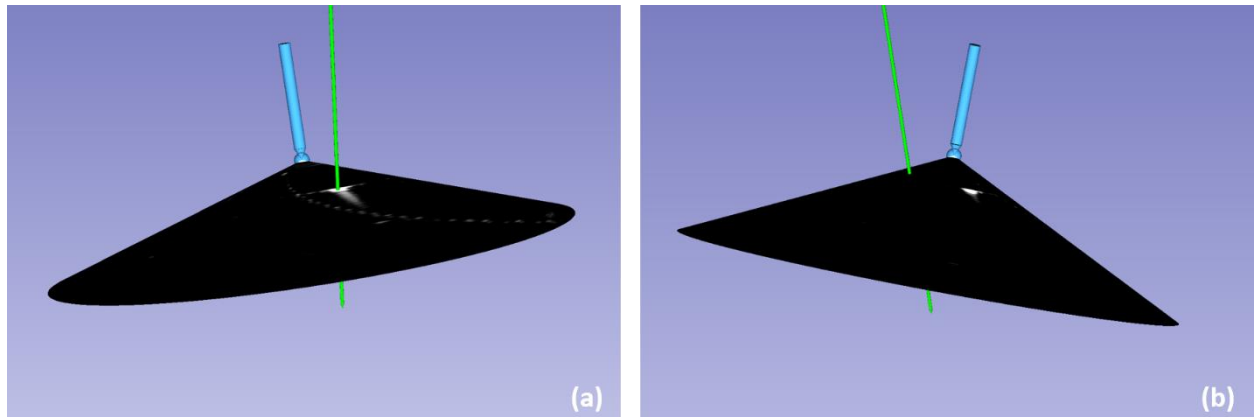


Figure 23 – (a) Slicer view of a tracked needle (virtual green line) intersecting its reflection in the ICE image right after calibration is performed, holding the ICE probe static. (b) Error introduced into the tracking environment when the probe is moved.

Mitigation

Due to the relative motion between the inner and outer layers of the ICE catheter, there are inaccuracies introduced into the tracking environment. This challenge adversely affects the design of any external tracking-based image-guided system. To address this limitation, an ideal solution would be to integrate the sensor on the innermost layer of the probe right next to the ultrasound transducer instead of the outer sheath. However, this solution requires a major redesign of the hardware which is outside the research scope of our lab.

To mitigate the challenge throughout the research and experiments performed, the probe was used with limited motion. The rest of the work presented in this thesis was designed to accommodate this limitation. Therefore, most experiments involve minimal to no linear probe movement. A small offset that might have been introduced in the time between ICE probe calibration and an experiment's data collection was corrected manually using the Transforms module in 3D Slicer.

Characterization of ICE Calibration

We performed spatial calibrations with the probe affixed in one position and varied the imaging angle. A calibration matrix was obtained with ultrasound images acquired at an angle (ϕ) of 50 degrees. Similarly, one calibration was performed for each of these imaging angles – 55, 60, 65, and 70 degrees. Immediately following each calibration, error metrics were computed as well.

The calibration procedure described previously, gives an error metric called fiducial localization error (FLE). To obtain a more realistic error metric i.e., target registration error (TRE), we used a point-based validation technique. The tip of a tracked and pre-calibrated 5DoF needle (NDI) served as the target point. The probe was fixed at one position and imaging angle, while the needle was carefully moved to its tip in the ultrasound image. The position of the needle tip in EM tracking space is compared to the position of its reflection as seen in the image, after application of the probe calibration and tracking information. The linear displacement between the two points provides one error or TRE value corresponding to one image. Multiple needle tip placements and associated ultrasound images furnish us with a series of validation points and TREs. We refer to this as a point-cloud validation technique.

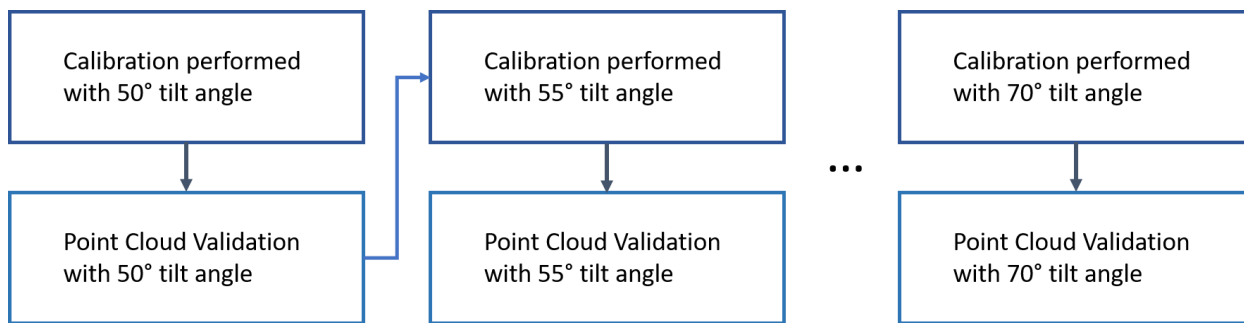


Figure 24 – Outline of experimental steps taken to collect data for the characterization of calibration and tracking behavior of the Foresight™ ICE probe.

A minimum of 8 different images, with reflections from the needle tip, were acquired with target points spread throughout the image plane. The entire process was repeated three times to assess the repeatability of the results. The probe was held constant within each trial, although the probe was re-plugged and moved after the first trial.

These experiments were performed to address several questions related to calibration specific to the forward-looking, radial, Foresight™ ICE probe. The questions are designed from both an R&D and clinical perspectives. These experiments test the repeatability of calibration, ideal imaging angle for calibration, radial distance and error relationship, and the angle-calibration error relationship as well. It should be noted that the study is post-hoc meaning that the questions were designed after the data were acquired and the data is not biased to favor any conclusion. Each section below describes the relevant questions, methods employed, results and the conclusion derived to answer those questions.

Repeatability of Spatial Calibration

In this section, we validated the spatial calibration technique by evaluating the repeatability of the calibration process for a single probe. The aim is to check the reliability of the calibration method with respect to a probe and answer the following question:

Is the process of spatial calibration valid and reliable for the Foresight ICE probe?

OR

Is the calibration/tracking accuracy consistent for multiple calibrations performed on the same probe?

Method: We tested the intra-probe variability of calibration accuracy by comparing the error metric TRE between the three trials. TRE was calculated by using the validation dataset acquired at 50 deg ICE imaging along with calibration performed at 50 deg (the same angle) and so on. The TREs from trials 1, 2, and 3 were compared to check whether they are significantly different from each other.

Result: The analysis of variance (ANOVA) testing for the errors among the three trials resulted in a p-value of 0.367 which means that we cannot reject the null hypothesis that the trials are similar. The box plot results are shown in the figure 25.

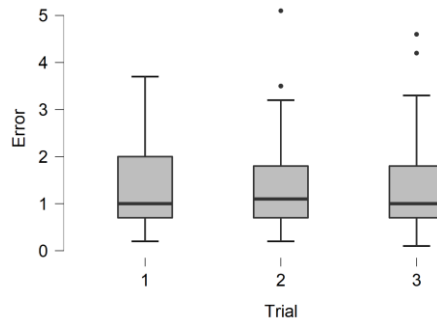


Figure 25 – Error distribution among the three trials.

Conclusion: The three boxes lie on the same horizontal line indicating that the three trials are not significantly different from each other. Based on this evaluation, we conclude the following:

The spatial calibration is reliable in terms of its repeatability for the same probe.

Intra-procedural positioning

In the radial Foresight ICE probe, smaller sized reflections are observed towards the center of the image or the apex of the cone, and wider needle reflections are seen towards the periphery. With respect to tracking, we want to determine whether the same behavior is observed with target registration error (TRE) as well. Clinically, it is important to know if measurements made in a tracked environment are more accurate when made in one portion of the image than the other. The clinical question becomes:

To make accurate measurements intraoperatively, should the targeted structure/anatomy be placed near the apex of the cone? OR

Is the effective error dependent on the radial distance from the center of the ICE image?

Method: To determine whether the TRE is a function of radial distance, we used the TRE information from the previous section. Since the three trials were similar, we combined the data from the three trials into one. For each TRE, there is an associated ultrasound image with a needle reflection. The radial distance is calculated between the apex of the cone (center of the image) and the centroid of the needle reflection. The TRE was plotted against the radial distance, and the significance of their relationship is evaluated using spearman's correlation coefficient. Spearman's rho was chosen over the Pearson's correlation coefficient since it is better at handling datasets with outliers and skewed variables. Spearman's alternative hypothesis is that the two variables are correlated.

Result: The TRE vs radial distance graph can be seen in figure 26. The graph itself shows no visible pattern or relationship between distance and error. Spearman's rho value is calculated to be 0.223 with a significance of $p < 0.01$, indicating that we can moderately accept the null hypothesis and reject the alternative hypothesis that the variables – TRE and radial distance are correlated.

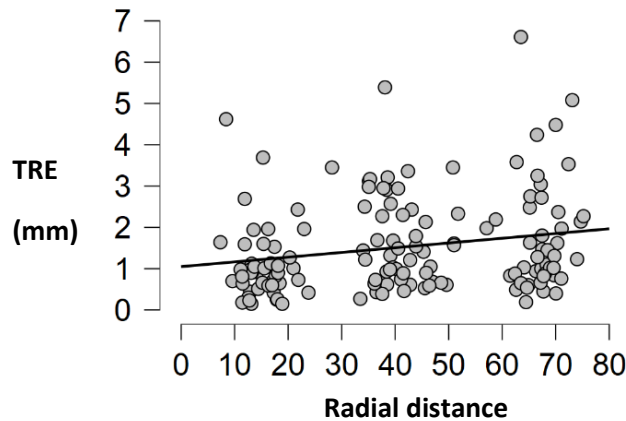


Figure 26 – Target registration error (vertical axis) plotted against the radial distance at which it was observed.

Conclusion: By observing Figure 26 and the correlation coefficient, we can conclude that there is no significant relationship between TRE and radial distance. Intraoperatively, measurements can be made freely as the errors introduced due to tracking are almost the same throughout the imaging plane. Thus we can answer the question as:

The effective error is independent of the radial distance from the center of the image. In a tracking environment, measurements made near the apex of the cone will not be significantly more accurate than those made at the periphery.

Calibration Uniformity wrt Imaging angle

Spatial calibration is a well-established procedure in literature, described and tested for planar ultrasound imaging. In the case of Conavi's Foresight ICE, there is another parameter involved, namely the angle of the cone or the imaging angle. When changing the imaging angle on the Foresight ICE probe, the angle of the cone itself changes but the apex of the cone remains at the same position. Since spatial calibration is performed with the origin of the image set to the apex of the cone, the calibration should be valid for imaging at all different angles. In this section, we evaluate whether the calibration performed at a specific angle is only valid for tracking images at that specific angle, or whether it can track ICE images acquired at other angles with the same accuracy.

If a probe is calibrated at a certain angle, is it suitable/accurate for ultrasound imaging only at that same angle? OR

Does a calibration matrix produce equally accurate tracking regardless of the imaging angle of the ICE?

These questions are of high clinical importance as they determine whether a clinician can freely switch between forward-looking and side-looking imaging with a tracked ICE probe and achieve the same level of accuracy.

Method: We use all the data collected for trials 2 and 3 in this study. Data from trial 1 could not be used due to a technical issue. For each calibration matrix acquired with imaging at a specific angle, the TRE is computed for all the available validation datasets with imaging performed at 50, 55, 60, 65, and 70 degrees. For each pair, we obtained a point cloud and then a set of TREs. The average TRE and standard deviation in error for each pair are represented in the form of a heatmap.

Result: Average TREs for each pair and the standard deviation in error for Trial 2 and Trial 3 can be seen in Figures 27 and 28 respectively.

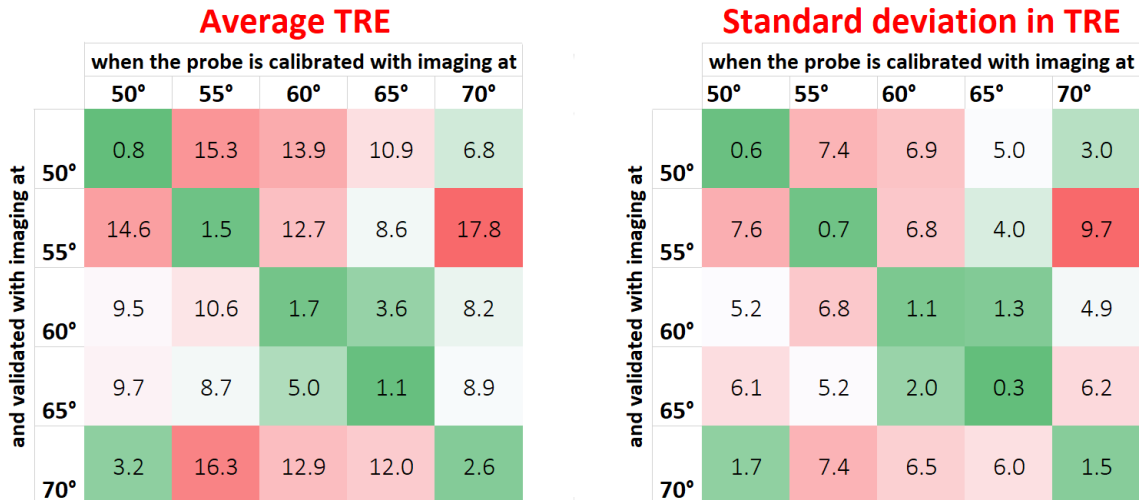


Figure 27 – (left) Average TRE and (right) standard deviation in TRE heatmaps when the probe is calibrated at a certain angle and validated with imaging at certain angles for Trial 2.

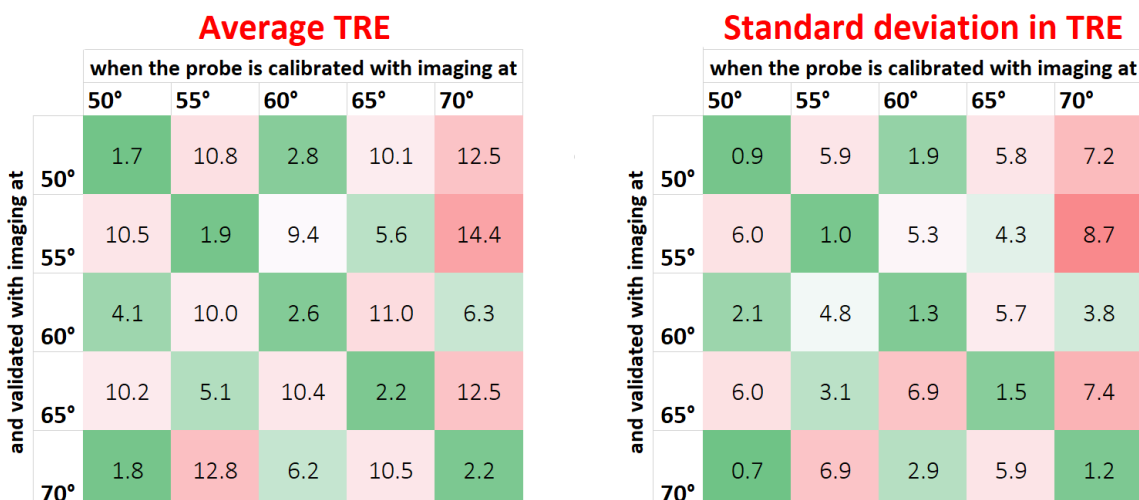


Figure 28 – (left) Average TRE and (right) standard deviation in TRE heatmaps when the probe is calibrated at a certain angle and validated with imaging at certain angles for Trial 3.

Conclusion: It can be seen in each of the four heatmaps that the diagonals are consistently green compared to the rest of the values, indicating that the TRE is minimum when the tilt angle of imaging is the same as that used during the calibration of the ICE probe. Therefore the answer to the question becomes:

The error is minimum when imaging is performed at the same angle at which the calibration was acquired. Thus, a calibration matrix is valid but might be less accurate when the imaging angle of ICE is different.

Tracking accuracy wrt Imaging Angle

From the previous section, we have established that tracked imaging is most accurate when acquired at the same imaging angle at which it was calibrated. In this section, we discuss the accuracy of tracked imaging in association with the imaging angle of the conical ultrasound. The Foresight ICE probe is considered more reliable and less noisy when imaged in a side-viewing mode rather than at a forward-looking angle. We investigate whether this trend is translated for tracked imaging as well. The question becomes:

Is there a relationship between target registration error and the angle at which it is calibrated?

OR

Is side-viewing imaging more accurate than forward-looking imaging?

Answering these questions will give a clinical context as to which angles to use to get the most accurate spatial information from the ultrasound.

Method: Since the data from the three trials are not significantly different (section 1 from this heading), we combined the TRE-angle dataset resulting in 135 samples in total. We used one-way ANOVA testing to determine whether there are any significant differences between the angle groups. The null hypothesis is “all the angle groups are the same”. A Tukey test was further conducted to determine where those differences may lie.

Result: Figure 29 shows the mean error for each of the angle groups along with a 95% confidence interval. Qualitatively, there is no visual pattern to observe. Testing with the entire dataset, the ANOVA results showed that there are statistically significant differences ($p < 0.05$) between the angle groups. The results of Tukey tests were unable to define which two angle pairs have significant differences between them since each angle pair had a $p_{tukey} > 0.05$.

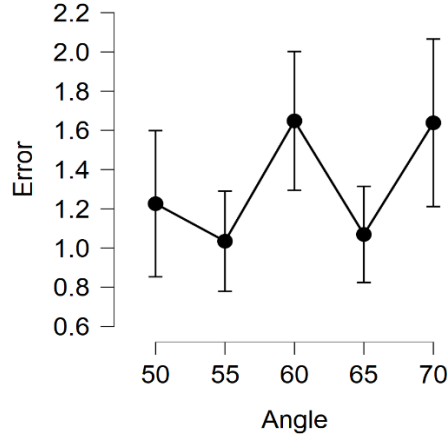


Figure 29 – Distribution of TRE with respect to imaging angle at which the ICE probe is calibrated and validated.

Conducting the ANOVA for the dataset without outliers, the results showed that there is no significant difference between any of the angle groups.

Conclusion: Due to the contradicting nature of the results it is difficult to draw any strong conclusions. However, the absence of any significant angle-pair from the Tukey test would indicate that the results of ANOVA using a full dataset may be biased due to the presence of outliers. Based on this assumption, we can conclude that

The tracking accuracy of an ICE probe is independent of the imaging angle used during a study.

Appendix A

Code for Conical Volume Reconstruction From a 2D Image

```

#
#
#----- Slicer function for Conical Image Reconstruction -----#
#
#
import slicer.util
import numpy as np
import math

def reconstruction(self, inputVolume, outputVolume, anglePhi):      #both
    volumes are scalar.
    phi = float(anglePhi)

    imgArr = slicer.util.arrayFromVolume(inputVolume)
    imgArr = np.squeeze(imgArr)
    Row, Col = imgArr.shape

    #Defining the origin/apex of the cone as the middle point of the image.

```

```

origin = ((int(Row/2), int(Col/2)))
edge   = ((Row, Col))

#Calculating the maximum value of z based on the max displacement of the
image from the center
# i.e from the middle of the image (cone apex) to the corner of the
image.
max_d = math.sqrt(sum( (edge - origin)**2 for edge, origin in zip(edge,
origin)))
max_z = max_d*math.tan(math.radians(90-phi))

#making an empty volume (choose an appropriate value of z)
vol = np.zeros((int(max_z+1), Row, Col), dtype=np.uint16)

#reconstruction: keeping x-axis and y-axis as same,
#calculation a height for each pixel value and populating volume
#origin(at apex) stays where it is, peripherals moved along z-axis.
result = np.where(imgArr) #get index of all voxels, for label map replace
imgArr==1
X = result[0] #row
Y = result[1] #col
D = np.sqrt((X-origin[0])**2 + (Y-origin[1])**2) # 6.6 us for X=
np.zeros(200)
Z = D*math.tan(math.radians(90-phi))
Z = Z.astype(int)
vol[Z,X, Y] = imgArr[X,Y]

#Update the volume(data) in the volume node with new array
slicer.util.updateVolumeFromArray(outputVolume, vol)

# -- Optional Volume Rendering --- #
volumeNode = outputVolume
slicer.util.updateVolumeFromArray(volumeNode, vol)
volRenLogic = slicer.modules.volumerendering.logic()
volRenWidget = slicer.modules.volumerendering.widgetRepresentation()
displayNode = volRenLogic.CreateDefaultVolumeRenderingNodes(volumeNode)
volumePropertyNode = displayNode.GetVolumePropertyNode()
volumePropertyNodeWidget = slicer.util.findChild(volRenWidget,
'volumePropertyNodeWidget')
volumePropertyNodeWidget.setMRMLVolumePropertyNode(volumePropertyNode)

return outputVolume

```

Code for Texture Mapping an Image to a Cone Model

```

#
#
#----- VTK-based, Slicer function for Texture Mapping -----#
#
#

```

```

import vtk, math

def textureMap(self, inputVolumeNode, anglePhi):
    dim = inputVolumeNode.GetImageData().GetDimensions()
    radius = int(dim[0]/2)
    height = radius*(math.tan(math.radians(90-anglePhi)))

    print("Texture Mapping function")
    print("Cone Angle is ", anglePhi, " Radius is ", radius, " and Height is "
    ", height)

    ##create a VTK coneSource / conical plane
    self.coneSource = vtk.vtkConeSource()
    self.coneSource.SetHeight(height)
    self.coneSource.SetRadius(radius)
    self.coneSource.SetResolution(100)

    #Center of the vtkConeSource is halfway up the height axis.
    #Actual origin should be at the apex of the cone/middle of circle
    self.coneSource.SetCenter(radius,radius, height/2)
    self.coneSource.CappingOff()
    self.coneSource.SetAngle(anglePhi)

    #This part defines the axis: the line drawn from the center of the base
    up towards the apex/vertex.
    self.coneSource.SetDirection(0,0,-1) # -z axis
    self.coneSource.Update()

    #Set the input image as teh texture
    self.texture = vtk.vtkTexture()
    self.texture.SetInputConnection(inputVolumeNode.GetImageDataConnection())

    #Set the cone source as the plane to be texture mapped
    self.texturePlane = vtk.vtkTextureMapToPlane()
    self.texturePlane.SetInputConnection(self.coneSource.GetOutputPort())

    #By default, the plane is centered at the origin and perpendicular to the
    z-axis,
    #with width and height of length 1 and resolutions set to 1.
    #Match the origin to the corner off of the cone and set two points at the
    other corners
    self.texturePlane.SetOrigin( 0, 0, 0)
    self.texturePlane.SetPoint1( 2*radius, 0, 0)
    self.texturePlane.SetPoint2( 0, 2*radius, 0)

    self.model = None
    if self.model is None:
        ##creating a new model in Slicer and set display properties
        self.model =
slicer.modules.models.logic().AddModel(self.texturePlane.GetOutputPort())
        self.model.SetName("Cone Model")
        self.modelDisp = self.model.GetDisplayNode()
        self.modelDisp.SetAmbient(1)
        self.modelDisp.SetDiffuse(1)
        self.modelDisp.SetSpecular(1)
        self.modelDisp.SetPower(1)
        self.modelDisp.SetFrontfaceCulling(0)

```

```

        self.modelDisp.SetBackfaceCulling(0)

    #Apply texture image to the plane (cone)

self.modelDisp.SetTextureImageDataConnection(inputVolumeNode.GetImageDataConnection())

    return self.model

```

Code for Volume Reconstruction from a DICOM file

```

#
#
#----- Slicer function for Image Reconstruction from DICOM --#
#
#
import scipy
from scipy import interpolate
import pydicom
import numpy as np
import math

def dicomReconstruction(self, filePath, outputVolumeNode, interpFactor,
interpEnabled):
    #fname =
'C:/Users/haree/Desktop/2.25.110163955407302945943070993686554932643.570.dcm'
    fname = filePath
    ds = pydicom.dcmread(fname)
    img = ds.pixel_array #numpy array with pixel data
    [row, col] = img.shape # [TH, R]
    R = img.shape[1] # or R = cols, (representing each echo along radius R)
    TH = img.shape[0] # or TH = rows (representing each theta)

    # Reading DICOM tags and extracting data
    phi = ds[0x15, 0x1000].value #float
    theta_en = ds[0x15, 0x1004].value #list #encoded [3,8... 1021]
    numFrames = ds[0x28, 0x0008].value # pydicom.valuerep.IS
    rows = ds[0x28, 0x0010].value #int (THETA)
    cols = ds[0x28, 0x0011].value #int (along RADIUS)
    spacing = ds[0x28, 0x0030].value #pydicom.multival.MultiValue
    TH_spacing= float(ds.PixelSpacing[0]) #float
    R_spacing = float(ds.PixelSpacing[1]) #float
    theta = theta_en/1024*360 # decoded theta values in degrees

    #----- interpolating -----
    if interpEnabled:
        print("DCM shape before interpolation: ", np.shape(img),
np.shape(theta), R, TH)
        rows2add = int(interpFactor) - 1
        [img, theta] = self.interpImage(img, theta, rows2add) #function to
interpolate img data before reconstruction
        R = img.shape[1] # or R = cols

```

```

TH  = img.shape[0] # or TH = rows
print("DCM shape after interpolation: ", np.shape(img),
np.shape(theta), R, TH)
#-----
#needed for spacing later
maxC, minC = 0, 2000

# Min size requirement of 3D volume is based on simple geometry (see
diagram)
[volx, voly, volz] = [2*R*math.sin(math.radians(phi)),
2*R*math.sin(math.radians(phi)), R*math.cos(math.radians(phi))]
vol = np.zeros((int(volx), int(voly), int(volz)), dtype=np.uint16)

[ox, oy, oz] = [round(volx/2), round(voly/2), 0]

vector = np.arange(0, TH)
sample = np.arange(0, R)

for v in vector:
    #getting polar angle theta for each vector
    th = theta[v]
    for s in sample:
        r = s*R_spacing #radial position for each sample
        #convert to cartesian
        a = r*math.sin(math.radians(phi))*math.cos(math.radians(th))
        b = r*math.sin(math.radians(phi))*math.sin(math.radians(th))
        c = r*math.cos(math.radians(phi))

        #scaling by 80(optimum number) to avoid overlappng or maybe FOV?
        a=int(round(a*80) + ox)
        b=int(round(b*80) + oy)
        c=int(round(c*80) + oz)

        # dicom image to volume pixel mapping
        vol[a,b,c] = img[v, s]

        if maxC < c:
            maxC = c
        if minC > c:
            minC = c

sp = R*R_spacing*10*math.cos(math.radians(phi))/(maxC-minC)

# update the volume(data) in the volume node with new array
slicer.util.updateVolumeFromArray(outputVolumeNode, vol)
outputVolumeNode.SetSpacing((sp,sp,sp)) # setting spacing using cone
geometry to ensure the radial length remains the same
outputVolumeNode.SetOrigin((0,0,0))
# now perform volume rendering through Slicer module

return outputVolumeNode

def interpImage(self, img, th, numRows):
#
#-----INTERPOLATING THETA VALUES -----

```

```

#
#Getting theta information from the original data, duplicating the last
row, and then upsampling theta array

TH = img.shape[0]
# th = decoded theta values in degrees
#2. Adding last row = first row (so that interpolation is on a closed
loop)
th = np.append(th, [th[0]+360])
TH += 1 #adding one to the total number of vectors TH=th.shape[0]

# 3. Upsampling theta values
interp_func = interpolate.interp1d(np.array(range(TH)), th, kind='linear',
axis=0)
R2add = numRows #e.g. 15 ROWS or VECTORS TO BE ADDED IN BETWEEN TWO
VECTORS
new_row = np.linspace(0, TH-1, R2add*(TH-1)+TH)
interp_th = np.array(interp_func(new_row))
TH = interp_th.shape[0]

# making sure that all theta values are under 360 (interpolation at the
end)
for i in range(TH-1-R2add , TH):#interp_th[-(R2add+1):]:
    if interp_th[i]>=360:
        interp_th[i] -= 360
    #end if
#end for

#
#----- INTERPOLATING IMAGE -----
#
# Before using interpolation on the rectangle image, copying the first
vector as an additional last vector
# because of cone geometry or loop - first and the last vector will
coincide now.

# Copy last row to end
img = np.concatenate((img, np.expand_dims(img[1,:], axis=0)), axis=0)
TH = img.shape[0]

# Upsampling - there is a duplicated last row which we will ignore in
reconstruction
interp_func = interpolate.interp1d(np.array(range(TH)), img,
kind='linear', axis=0)

# ROWS or VECTORS TO BE ADDED IN BETWEEN TWO VECTORS (must be same as
before)
new_row = np.linspace(0, TH-1, R2add*(TH-1)+TH)
interp_img = np.array(interp_func(new_row))
TH = interp_img.shape[0]

return interp_img, interp_th

```